

Asteroid Deflection Using a Spacecraft in Restricted Keplerian Motion

Yohannes Ketema

Dept. of Aerospace Engineering and Mechanics
University of Minnesota, Minneapolis, MN 55455

March 6, 2022

Abstract

A method for asteroid deflection that makes use of a spacecraft moving back and forth on a segment of a Keplerian orbit about the asteroid is described and studied. It is shown that on average the spacecraft can exert a significantly larger force on the asteroid than e.g. a stationary gravity tractor, thereby reducing the time needed to effect the desired deflection of the asteroid. Furthermore, the current method does not require canted thrusters on the spacecraft (unlike a stationary gravity tractor) markedly reducing the amount of fuel needed for a given deflection to be realized. The method also allows for the simultaneous use of several spacecraft, further strengthening the overall tugging effect on the asteroid, and distributing the thrust requirement among the spacecraft.

Nomenclature

m_a	=	mass of asteroid
m_c	=	mass of spacecraft
μ_a	=	gravitational parameter for asteroid
μ_c	=	gravitational parameter for spacecraft
r_a	=	radius of asteroid
r	=	distance to spacecraft from asteroid center
α	=	ratio of spacecraft distance to asteroid radius
G	=	universal gravitational constant
θ	=	true anomaly on spacecraft orbit about asteroid
θ_b	=	bounding angle on spacecraft orbit about asteroid
Δv	=	impulsive velocity change
I	=	impulse imparted to asteroid
h	=	specific angular momentum for spacecraft orbit about asteroid
r_p	=	periapsis distance for spacecraft orbit about asteroid
r_{pm}	=	smallest allowable periapsis distance for spacecraft orbit about asteroid
e	=	eccentricity of spacecraft orbit about asteroid
γ	=	flight path angle for spacecraft orbit about asteroid
φ	=	plume half angle
v_{esc}	=	escape velocity for motion with respect to asteroid
t_m	=	time of flight on spacecraft orbit segment
$\eta_k(\theta_b, \varphi, e)$	=	nondimensional average force from spacecraft in orbit
$\eta_k(\theta_b, \varphi)$	=	nondimensional average force from spacecraft in circular orbit
η_s	=	nondimensional average force from stationary gravity tractor
β	=	angle between asteroid-spacecraft vector and line from spacecraft tangent to the asteroid surface
f_{do}	=	force exerted on asteroid by spacecraft in displaced orbit
$\zeta_k(\theta_b, e)$	=	nondimensional impulse per unit mass of fuel used in orbiting spacecraft
ζ_s	=	nondimensional impulse per unit mass of fuel used in stationary spacecraft
$\nu(\theta_b, e, \varphi)$	=	nondimensional impulsive velocity change

1 Introduction

The potential for Earth-asteroid impacts [1, 2] has recently generated much interest in the development of techniques to avert a projected collision by modifying the orbit of the asteroid. A broad study of possible approaches to the deflection of asteroids is presented in [4] where various methods are compared, and an assessment is made of their technology readiness. Asteroid deflection schemes analyzed include nuclear interceptors, kinetic impactors, and gravity tractors.

Nuclear interceptors are meant to detonate a nuclear charge on or at a distance from the surface of an asteroid [4–7]. When considering asteroid deflection using a nuclear charge, it is important to take into account the response of the asteroid body to the nuclear detonation, i.e. whether it might break up into small fragments, or if the asteroid will remain a single body, which would be the ideal case. Therefore, the material composition of the asteroid and its structural characteristics are important factors that must be studied. It has been shown [4] that the distance from the surface of the asteroid to the detonating nuclear charge can be used as a parameter to effect the latter

scenario.

Kinetic impactors aim to impart an impulse to the asteroid through a direct collision. Studies of kinetic impactors can be found in [5, 8–11]. As in the case of nuclear interceptors, careful consideration must be given to the composition of the asteroid to ensure that it does not break up during the collision.

A method of asteroid deflection that is unaffected by the composition of the asteroid is the gravity-tractor, where a spacecraft exerts a force on the asteroid purely through gravitational coupling. Since the gravity tractor was first proposed in [12] it has been the subject of several studies on topics such as the optimal control of its position with respect to the asteroid, and realistic studies of implementation for the deflection of specific asteroids [13–16].

In its basic form (as will be detailed further in the body of this paper) the gravity tractor uses a pair of thrusters that are canted with respect to the direction of the force to be exerted on the asteroid. This is necessary so that exhaust plumes do not impinge on the asteroid directly, as this would counteract the gravitational tugging effect. However, the canting of the thrusters means that a considerable amount of thrust goes unused in terms of asteroid deflection, making the gravity tractor rather inefficient with respect to fuel use.

A gravity tractor that does not necessarily require canted thrusters has been suggested in [17] where the spacecraft is in a displaced non-Keplerian orbit with respect to the asteroid. It is shown that when the offset distance of the orbit from the center of the asteroid is sufficiently large (to avoid plume impingement), this method can produce the same magnitude of net force on the asteroid as the stationary gravity tractor, for a 25% less thrust developed by the spacecraft’s thruster. The requirement of relatively large offset distances, however, means that the force from the displaced-orbit gravity tractor is generally small – in the same order of magnitude as that of the stationary gravity tractor. Also, for the values of the offset required to avoid plume impingement, the displaced orbit is unstable as follows from the analysis in [18], and must be stabilized using state feedback.

The use of formation flying spacecraft in displaced non-Keplerian orbits with solar sails, and associated problems of controlling the formation are studied in [19]. This approach, while similar to the displaced-orbits-method in [17] removes the problem of plume impingement.

A common characteristic of the above mentioned approaches to asteroid deflection is that the perturbing forces applied on the asteroid are generally small (compared to the force of gravity from the Sun on the asteroid). However, as shown in [3], the effect of these perturbing forces on the resulting deflection increases with passing time through a secular effect. Thus it is advantageous to start the deflection action as early as possible before the projected time of collision. On the other hand, the amount of time available between the detection of an asteroid and the projected time of collision may not be large. It is therefore important to study ways of increasing the forces that are exerted on the asteroid, regardless of what specific method is being used.

The main goal of the current paper is therefore to present a gravity tractor that on average can exert a significantly larger force on the asteroid than the gravity-based methods mentioned above, for the same spacecraft mass. In this method the spacecraft describes what will be referred to as *restricted Keplerian motion* about the asteroid. The motion, as will be described further in the body of this paper, consists of the spacecraft moving back and forth along a segment of a Keplerian orbit, changing the direction of its velocity at the ends of the segment through impulsive thrusts. In addition to the larger average force exerted on the asteroid when using the current method, the net impulse on the asteroid per mass of fuel used in the spacecraft is significantly larger than in the case of the stationary gravity tractor. This translates into higher efficiency in terms of deflection

effected per amount of fuel used. The advantages gained in a larger average force and increased impulse per mass, compared to other gravitationally based methods, derive from the fact that the spacecraft can generally come closer to the surface of the asteroid while saving fuel by not having to use canted thrusters.

The rest of this paper is organized as follows: In Section 2 the forces on the asteroid-spacecraft system are identified and the equations of motion for the asteroid and for the spacecraft are written. In Section 3 an expression for the deflection of the asteroid is derived in terms of the characteristics of the restricted Keplerian motion. Next in Section 4, the force exerted by the gravity tractor on the asteroid is studied and compared to the corresponding forces from a stationary gravity tractor and a displaced-orbit gravity tractor for a given spacecraft mass. The performance of the gravity tractor from the point of view of fuel expenditure is studied in Section 5, where a measure of fuel efficiency is defined and compared between the current gravity tractor, the stationary gravity tractor, and the displaced-orbit gravity tractor. A numerical example is presented in Section 6 where a hypothetical deflection of Asteroid 2007 VK184 is studied and compared to existing results using other methods. Lastly, concluding remarks are given in Section 7.

2 Forces on the asteroid

Consider a spacecraft flying near an asteroid in a known orbit about the Sun as shown schematically in Figure 1. In the figure, the position vector from the Sun to the asteroid is denoted by \mathbf{R} , the position vector from the asteroid to the spacecraft is denoted by \mathbf{r} , and the position vector from the Sun to the spacecraft is denoted by \mathbf{R}_c . The gravitational forces from the Sun on the asteroid and from the spacecraft on the asteroid are denoted by \mathbf{F}_{as} and \mathbf{F}_{ac} , respectively. The spacecraft is subjected to the gravitational forces \mathbf{F}_{ca} and \mathbf{F}_{cs} from the asteroid and the Sun, respectively. In addition, a propulsive force \mathbf{T} may act on the spacecraft from its own thruster. Denoting the magnitudes of the vectors \mathbf{R} , \mathbf{r} , and \mathbf{R}_c by R , r and R_c , respectively, the gravitational forces may be written as

$$\mathbf{F}_{as} = -\frac{Gm_a m_s}{R^3} \mathbf{R} \quad (1)$$

$$\mathbf{F}_{ac} = \frac{Gm_a m_c}{r^3} \mathbf{r} \quad (2)$$

$$\mathbf{F}_{ca} = -\frac{Gm_c m_a}{r^3} \mathbf{r} \quad (3)$$

$$\mathbf{F}_{cs} = -\frac{Gm_c m_s}{R_c^3} \mathbf{R}_c \quad (4)$$

$$(5)$$

where m_s , m_a , and m_c are the masses of the Sun, the asteroid, and the spacecraft, respectively, and G is the universal gravitational constant. It should be noted that the mass of the spacecraft is time dependent, as it decreases with the burning of fuel.

2.1 The center of mass of the asteroid-spacecraft system

In the following study of the effects of the forces on the asteroid-spacecraft system in Figure 1, it will be useful to take into account the location of the center of mass of the system. Thus the

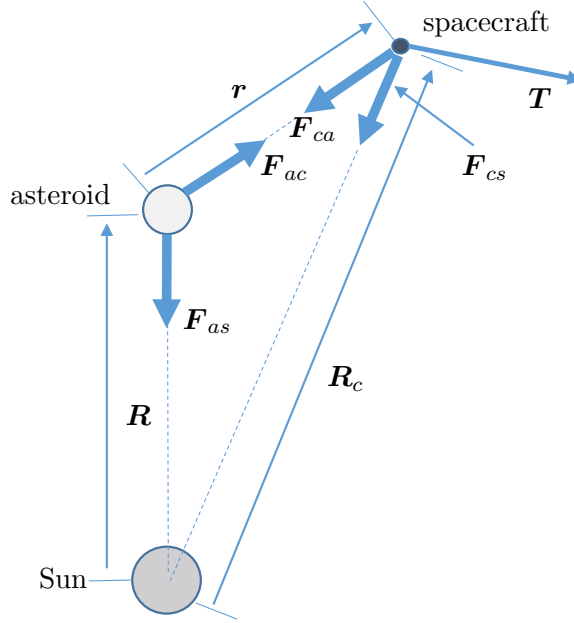


Figure 1: The asteroid-spacecraft system.

position of the center of mass of the asteroid-spacecraft system, with respect to the center of the asteroid, may be expressed as

$$\mathbf{r}_G = \frac{m_c}{m_a + m_c} \mathbf{r}, \quad (6)$$

where \mathbf{r} is defined in Figure 1. When the mass of the spacecraft is much smaller than that of the asteroid ($m_c \ll m_a$), which will be assumed in what follows, the center of mass of the system will be very close to the center of mass of the asteroid. To get a sense for the typical distances involved, it is useful to consider an example. Following [12] we consider a hypothetical asteroid of diameter 100 m and mass 8.4×10^9 kg. Suppose that a spacecraft of mass 2000 kg is at a distance of 100 m from the center of the asteroid. It would follow from (6) that the center of mass is at a distance of $r_G = 2.4 \times 10^{-5}$ m from the center of the asteroid. In general, we conclude that when $m_c \ll m_a$ the center of mass of the system may be considered to be at the center of mass of the asteroid. An analysis of the deflection of the asteroid may therefore be based on either the motions of the center of mass of the asteroid itself, or equivalently, on the motions of the center of mass of the asteroid-spacecraft system. In this paper the former approach will be taken.

2.2 The thrust as an external force to the asteroid-spacecraft system

It is suggested in Figure 1 that the thrust T only acts on the spacecraft and is therefore an external force to the asteroid-spacecraft system. This would not be true if the generation of the thrust involved an interaction with the asteroid (for example through significant forces between the exhaust gases and the asteroid). It is therefore important to validate this basic assumption that the thrust T is indeed an external force to the system.

We first consider the thrust T from the point of view of its action on the spacecraft using a control volume approach [20]. Thus we define a volume V_1 that encompasses the spacecraft as

shown in Figure 2(a). The rate of change of momentum inside the control volume can be related to the net force on the mass inside the control volume (i.e. the total gravitational force on the spacecraft, say \mathbf{F}_c) and the rate at which mass flows in or out of the control volume. This leads to the equation

$$\mathbf{F}_c = \frac{d}{dt} \int_{V_1} \rho \mathbf{v} dV + \int_{A_1} \rho \mathbf{v} (\mathbf{v}_r \cdot d\mathbf{A}) \quad (7)$$

where \mathbf{F}_c is the total external force on the spacecraft given by

$$\mathbf{F}_c = -\frac{Gm_a m_c}{r^3} \mathbf{r} - \frac{Gm_s m_c}{R_c^3} \mathbf{R}_c, \quad (8)$$

and $\int_{V_1} \rho \mathbf{v} dV$ is the total momentum of all particles within the control volume, i.e. the spacecraft. The area A_1 is the surface area of the control volume V_1 and \mathbf{v}_r is the component of the velocity of the exhaust gases in a direction perpendicular to an area element $d\mathbf{A}$, with respect to the area element. The velocity \mathbf{v}_r is defined positive if it corresponds to a flow of gases out of the control volume.

The total momentum of the mass m_c inside the control volume can also be written in terms of the velocity of its center of mass \mathbf{v}_c , i.e.

$$m_c \mathbf{v}_c = \int_{V_1} \rho \mathbf{v} dV \quad (9)$$

Rearranging the terms in (7) and using (9) we have

$$\frac{d}{dt} (m_c \mathbf{v}_c) = \mathbf{F}_c - \int_{A_1} \rho \mathbf{v} (\mathbf{v}_r \cdot d\mathbf{A}) \quad (10)$$

or

$$m_c \frac{d\mathbf{v}_c}{dt} = \mathbf{F}_c - \int_{A_1} \rho \mathbf{v} (\mathbf{v}_r \cdot d\mathbf{A}) - \frac{dm_c}{dt} \mathbf{v}_c \quad (11)$$

where the last two terms on the right hand side represent the thrust from the rocket, i.e.

$$\mathbf{T} = - \int_{A_1} \rho \mathbf{v} \mathbf{v}_r \cdot d\mathbf{A} - \frac{dm_c}{dt} \mathbf{v}_c \quad (12)$$

Once the exhaust gases are ejected from the spacecraft, they move at a very large velocity with respect to the asteroid and out of the *SOI*, as will be demonstrated by example below. Due to the low density, and therefore small amount of total mass of gas within the *SOI* at any time, the gravitational effect of the gases on the asteroid can be neglected (just as their gravitational effects on the spacecraft may be neglected). With this in mind, we next consider a larger control volume V_2 , as in Figure 2b, which consists of V_1 and an additional part that encompasses the asteroid. We can relate the total gravitational force on the asteroid-spacecraft system to the rate of change of the momentum inside the control volume in the form

$$\mathbf{F} = \frac{d}{dt} \int_{V_2} \rho \mathbf{v} dV + \int_{A_2} \rho \mathbf{v} (\mathbf{v}_r \cdot d\mathbf{A}) \quad (13)$$

where A_2 is the total surface area of the control volume V_2 and \mathbf{F} is the total external gravitational force on the asteroid-spacecraft system or

$$\mathbf{F} = -\frac{Gm_a m_s}{R^3} \mathbf{R} - \frac{Gm_c m_s}{R_c^3} \mathbf{R}_c \quad (14)$$

Again the momentum within V_2 (i.e. the spacecraft and the asteroid) may be written as

$$\int_{V_2} \rho \mathbf{v} dV = m_a \mathbf{v}_a + m_c \mathbf{v}_c \quad (15)$$

Using (13) and (15), and noting that m_a is constant we have

$$m_a \frac{d\mathbf{v}_a}{dt} + m_c \frac{d\mathbf{v}_c}{dt} = \mathbf{F} - \int_{A_2} \rho \mathbf{v} (\mathbf{v}_r \cdot d\mathbf{A}) - \frac{dm_c}{dt} \mathbf{v}_c \quad (16)$$

or denoting the velocity of the center of mass of the asteroid-spacecraft system by \mathbf{v}_G

$$(m_a + m_c) \frac{d\mathbf{v}_G}{dt} = \mathbf{F} - \int_{A_2} \rho \mathbf{v} (\mathbf{v}_r \cdot d\mathbf{A}) - \frac{dm_c}{dt} \mathbf{v}_c \quad (17)$$

where the last two terms on the right hand side constitute the thrust that is generated on the asteroid-spacecraft system due to the ejection of mass out of the volume V_2

$$\mathbf{T}_{syst} = - \int_{A_2} \rho \mathbf{v} (\mathbf{v}_r \cdot d\mathbf{A}) - \frac{dm_c}{dt} \mathbf{v}_c \quad (18)$$

Noting that, from a physical point of view, the integrals in (12) and (18) are identical leads to the conclusion that

$$\mathbf{T} = \mathbf{T}_{syst} \quad (19)$$

and the thrust acting on the spacecraft can therefore be considered an external force on the system that has the ability to perturb the motion of the center of mass of the system about the Sun.

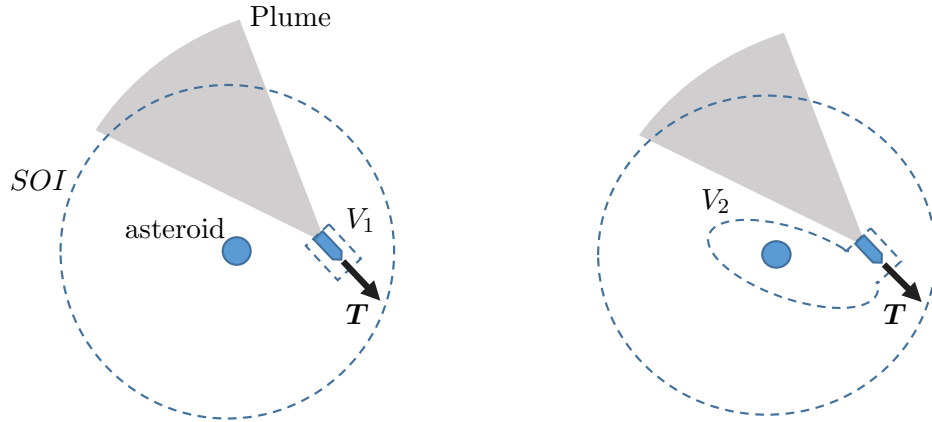


Figure 2: The asteroid-spacecraft system and control volumes.

To further justify the assumption that the exhaust gases leave the *SOI* of the asteroid largely unaffected by the asteroid, it may be useful to study an example. We consider again an asteroid of diameter 100 m and mass 8.4×10^9 kg. The magnitude of the velocity of the exhaust with respect to the spacecraft from a rocket of specific impulse I_{sp} can be found from (see e.g. [20])

$$v_{e/c} = g I_{sp} \quad (20)$$

where $g = 9.81 \text{ m/s}^2$ is the acceleration due to gravity on the surface of Earth. Thus for example with $I_{sp} = 200 \text{ s}$

$$v_{e/c} = 1962 \text{ m/s} \quad (21)$$

The velocity of a spacecraft in a circular orbit about the asteroid at a radius of $r = 75 \text{ m}$ would be

$$v = \sqrt{\frac{\mu}{r}} = 0.09 \text{ m/s}, \quad (22)$$

therefore not significantly adding to the velocity of the exhaust.

On the other hand, the escape velocity near the surface of the asteroid considered is

$$v_{esc} = \sqrt{\frac{2\mu}{r}} \quad (23)$$

or

$$v_{esc} = 0.15 \text{ m/s} \quad (24)$$

It is therefore clear that,

$$v_e \gg v_{esc} \quad (25)$$

due to the very large velocity of the exhaust, it can always be expected to exit the *SOI* of the asteroid without further interaction with the asteroid.

Another force that in principle could be acting on the asteroid but that is not included in the free body diagrams in Figure 1 is a direct force from the exhaust plume from the spacecraft's thruster on the asteroid. This force may exist if the exhaust plume impinges on the asteroid, thus counteracting the effect of the gravitational force from the spacecraft on the asteroid. In practice, this scenario can be easily avoided by imposing a constraint on the possible directions of the thrust T , and only allowing those directions that do not lead to plume impingement, as is suggested for example, in Figure 2.

2.3 Equations of motion

Considering the free body diagrams in Figure 1, the equation of motion for the asteroid and the spacecraft in the inertial frame may be written as

$$m_c \ddot{\mathbf{R}}_c = \mathbf{F}_{cs} + \mathbf{F}_{ca} + \mathbf{T} \quad (26)$$

$$m_a \ddot{\mathbf{R}} = \mathbf{F}_{as} + \mathbf{F}_{ac} \quad (27)$$

From (27) it follows that the perturbing force on the asteroid that will be responsible for a modification of its orbit is \mathbf{F}_{ac} , i.e. the gravitational force from the spacecraft. In particular, the thrust \mathbf{T} does not directly affect the motions of the asteroid. However, it serves the important purpose of controlling the motions of the spacecraft with respect to the asteroid, and therefore controlling the magnitude and direction of \mathbf{F}_{ac} . (See for example [15] for the alternative approach of considering the motions of the center of mass of the system and where \mathbf{T} is the force that modifies the orbit of the center of mass.)

3 The asteroid deflection formula

The equation of motion for the asteroid (27) is in the general form

$$\frac{d\mathbf{p}}{dt} = \mathbf{F}_{as} + m_a \mathbf{A}(t) \quad (28)$$

where \mathbf{p} is the momentum of the asteroid and $\mathbf{A}(t)$ is defined so that

$$\mathbf{F}_{ac} = m_a \mathbf{A}(t) \quad (29)$$

or

$$\mathbf{A} = \frac{Gm_c}{r^3} \mathbf{r} \quad (30)$$

The vector $\mathbf{A}(t)$ may thus be interpreted as the perturbing acceleration on the asteroid that is caused by the gravitational force from the spacecraft.

Denoting the time of projected encounter between Earth and the asteroid by t_e , the goal for the acceleration \mathbf{A} is to effect a non-zero distance of closest approach (i.e. a deflection) between the Earth and the asteroid at that time. This distance is described in Figure 3 where it is denoted by $\Delta\zeta$ and measured in a direction perpendicular to the velocity of the asteroid with respect to Earth.

In general, the distance $\Delta\zeta$ at time t_e will depend on the time $t_s < t_e$ when the perturbing acceleration \mathbf{A} begins to act and the time $t_f \leq t_e$ at when stops acting. An expression for $\Delta\zeta$ known as the asteroid deflection formula is derived in [3] and takes the form

$$\Delta\zeta = \frac{3a}{\mu} v_a(t_e) \sin \psi \int_{t_s}^{t_f} (t_e - t) \mathbf{v}_a \cdot \mathbf{A}(t) dt \quad (31)$$

where \mathbf{v}_a is the time dependent heliocentric velocity of the asteroid, $v_a(t_e)$ is the magnitude of the asteroid's velocity at the time of the projected encounter, and ψ is the angle between the heliocentric velocity of the asteroid and its relative velocity with respect to Earth (see Figure 3). Using (30) it follows that

$$\Delta\zeta = \frac{3a}{\mu} v_a(t_e) \sin \psi \int_{t_s}^{t_f} (t_e - t) \mathbf{v}_a \cdot \frac{Gm_c}{r^3} \mathbf{r} dt \quad (32)$$

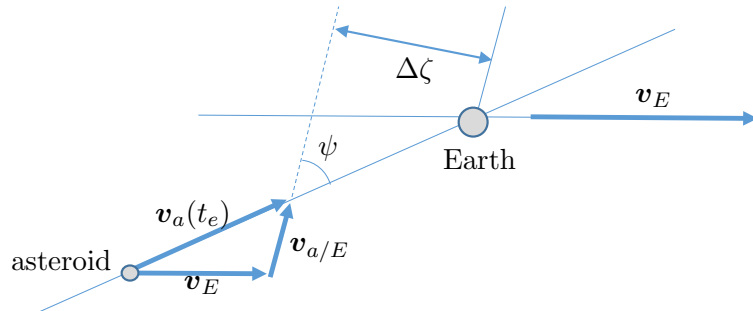


Figure 3: Earth and the asteroid at the time of closest approach.

Note that $\Delta\zeta$ can be positive or negative depending on the time history of $\mathbf{v}_a \cdot \mathbf{A}$. The case $\Delta\zeta > 0$ implies that the asteroid arrives at the projected point of collision with Earth, after the Earth has passed that point. This is the case depicted in Figure 3. On the other hand, $\Delta\zeta < 0$ would mean that the asteroid passes the projected point of collision before the Earth arrives at that point. Apart from the resulting sign of $\Delta\zeta$ there is no difference in how these two cases are analyzed. In what follows we will assume that the required deflection is $\Delta\zeta < 0$. Thus it follows from (31) that \mathbf{A} should be directed so that $\mathbf{v}_a \cdot \mathbf{A} < 0$. In other words, the component of the gravitational force from the spacecraft on the asteroid should act so as to oppose the heliocentric motion of the asteroid.

Figure 4 illustrates the action of the gravitational force from the spacecraft on the asteroid in relation to the direction of the asteroid's velocity, which is assumed to be pointing to the left in the figure. The x axis is defined to point in a direction opposite to the heliocentric velocity of the asteroid \mathbf{v}_a and the y axis points in a direction perpendicular to x and lies in the plane of the asteroid's orbit. Denoting the x component of the gravitational force \mathbf{F}_{ac} by F_{acx} , and recalling (30) the condition that $\mathbf{v}_a \cdot \mathbf{A} < 0$ is equivalent to $F_{acx} > 0$. In terms of the angle θ between \mathbf{F}_{ac} and the x axis, it is required that $|\theta| < \frac{\pi}{2}$.

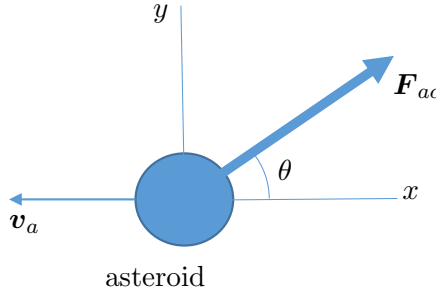


Figure 4: The gravitational force from the spacecraft on the asteroid in relation to the direction of the heliocentric velocity of the asteroid.

Of course, the direction of the gravitational force \mathbf{F}_{ac} is determined by the position of the spacecraft with respect to the asteroid as this force always points toward the spacecraft. This implies that the spacecraft should always be in the right half of the xy plane as defined in Figure 4. In the next section, it will be described how the spacecraft can maintain this type of motion.

3.1 Restricted Keplerian Motion

When the spacecraft is within the sphere of influence (SOI) of the asteroid, its motion with respect to the asteroid may be studied using the two-body model. It is then well known that any unforced motion will take place along a conic section (ellipse, parabola, or hyperbola) that will generally visit both halves of the plane. Thus, in order to keep the spacecraft in the right half plane, so that $|\theta| < \pi/2$ in Figure 4, it will be necessary to restrict its motion by imparting intermittent impulsive velocity changes Δv . In this way, the spacecraft can be made to move along a segment of a conic section in alternating directions. Figure 5 shows two examples of such motion. In Figure 5(a) the spacecraft moves back and forth along an elliptic orbit, and in Figure 5(b) the spacecraft moves back and forth along a hyperbolic orbit. A similar motion is of course possible along a parabolic

orbit as well. The changes in velocity Δv qualitatively depicted in Figure 5 are imparted through the action of the thrust \mathbf{T} on the spacecraft. In what follows, the motion of the back and forth motion of the spacecraft as described above will be referred to as “restricted Keplerian motion” and the corresponding gravity tractor will be referred to as a “Keplerian” gravity tractor.

It is worth noting that the Δv 's required for such motions around large objects such as planets would be prohibitively large due to the generally large velocities of the spacecraft that would be needed. The orbital velocities around an asteroid, on the other hand, are generally small as has been exemplified in (22) making this restricted Keplerian motion plausible.

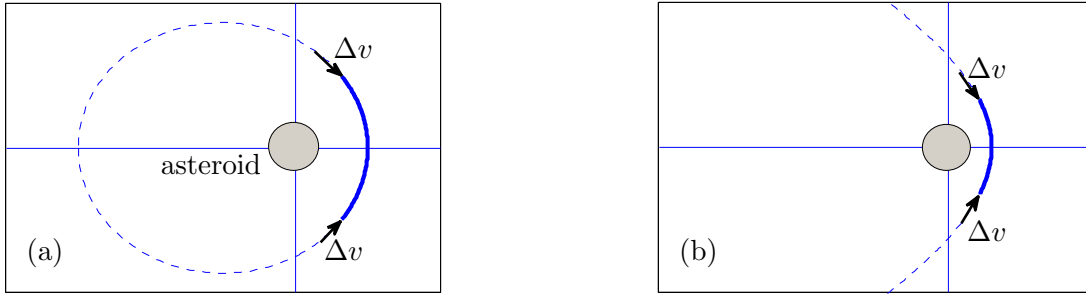


Figure 5: Schematic illustration of restricted Keplerian motion: (a) on an elliptic orbit, (b) on a hyperbolic orbit.

3.2 An expression for the resulting deflection: the average force

While Figure 5 describes qualitatively the motion of the spacecraft with respect to the asteroid, the orbit itself, as defined by its parameters such as semimajor axis and eccentricity, and the length of the segment on the orbit along which the spacecraft will travel, will influence the overall deflecting effect of the gravitational force from the spacecraft. The dependence of the performance of the gravity tractor on these parameters will be studied in this and the following sections.

Figure 6 depicts schematically a segment of a generic conic section along which the spacecraft flies back and forth in a restricted Keplerian motion. Thus the spacecraft flies from point A to point B , then back to point A etc. This motion is made possible through impulsive thrusts Δv_1 and Δv_2 that change the direction of the velocity of the spacecraft at points A and B , respectively. The maximum $|\theta|$ at which the impulsive thrusts are delivered will be denoted by θ_b and will be referred to as the bounding angle in what follows.

The time it takes the spacecraft to go from point A to point B , or subsequently from point B to point A , can be calculated using the time of flight formulas for the two body problem (see Section 4). Here we just note that the time is independent of the direction of motion and only depends on the bounding angle θ_b and parameters of the given conic section, namely the semimajor axis and eccentricity.

The total deflection caused by this back and forth motion can be calculated using the deflection formula (32). With the help of Figure 6 we note that

$$\mathbf{v}_a \cdot \frac{Gm_c}{r^3} \mathbf{r} = -v_a \frac{Gm_c}{r^2} \cos \theta \quad (33)$$

where v_a is the (generally time dependent) magnitude of \mathbf{v}_a . Using this expression in (32) leads to

$$\Delta\zeta = -\kappa \int_{t_s}^{t_f} (t_e - t) v_a \frac{Gm_c}{r^2} \cos \theta dt, \quad (34)$$

where we have defined for brevity

$$\kappa = \frac{3a}{\mu} v_a(t_e) \sin \psi \quad (35)$$

To evaluate the integral in (38) we note that the interval of integration $[t_s, t_f]$ may be broken up into smaller intervals, each corresponding to one pass of the spacecraft along the orbit segment in Figure 6, either going from A to B or from B to A . Suppose that there are N such passes on the orbit segment during the time interval $[t_s, t_f]$. The successive times at which the spacecraft reaches the endpoints of the orbit segment may then be denoted by $t_i : i = 1, 2, \dots, t_{N+1}$ where $t_1 = t_s$ (the initial time), $t_{N+1} = t_f$, and

$$t_{i+1} = t_i + \Delta t \quad (36)$$

where Δt is the time of flight between points A and B . It then follows that the integral in (34)

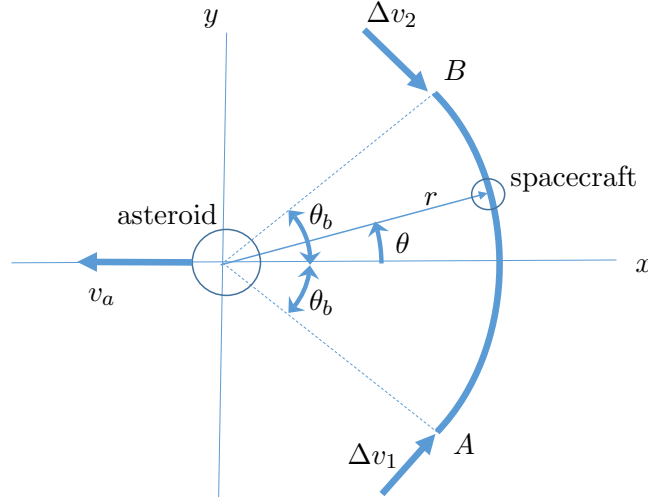


Figure 6: The asteroid-spacecraft system.

may be written as

$$\Delta\zeta = \sum_{i=1}^N \Delta\zeta_i \quad (37)$$

where $\Delta\zeta_i$ is the contribution to $\Delta\zeta$ from the time interval $[t_i, t_{i+1}]$ that is given by

$$\Delta\zeta_i = -\kappa \int_{t_i}^{t_{i+1}} (t_e - t) v_a \frac{Gm_c}{r^2} \cos \theta dt, \quad (38)$$

Note that the mass of the spacecraft m_c is constant within the time interval $[t_i, t_{i+1}]$ as the Δv 's are executed at the times t_i . This constant mass in the time interval $[t_i, t_{i+1}]$ will be denoted by

m_{ci} . Also, the integrand in (38) can be simplified by using the definition of the magnitude of the angular momentum for the spacecraft about the asteroid (see e.g. [22, 23])

$$h = r^2|\dot{\theta}|, \quad (39)$$

Using (39) and the constant mass of the spacecraft m_{ci} in (38) leads to

$$\Delta\zeta_i = -\kappa \int_{t_i}^{t_{i+1}} (t_e - t) v_a \frac{Gm_{ci}}{h} \cos \theta |\dot{\theta}| dt, \quad (40)$$

Suppose now that in a time interval $[t_i, t_{i+1}]$ the spacecraft is moving along the orbit segment in the counterclockwise direction, i.e. $\dot{\theta} > 0$. Then the true anomaly θ will vary from $\theta = -\theta_b$ to $\theta = \theta_b$. In this case, (40) may be written

$$\Delta\zeta_i = -\kappa \int_{t_i}^{t_{i+1}} (t_e - t) v_a \frac{Gm_{ci}}{h} \cos \theta \dot{\theta} dt, \quad (41)$$

To further simplify (41), we consider the order of magnitude of the time interval $[t_i, t_{i+1}]$. Thus revisiting the asteroid-spacecraft system described at the end of Section 2.2, we note that the time it would take the spacecraft to fly through an angle of π radians, for example, along a circular orbit of radius of $r=100$ m would be (see e.g. [24])

$$\Delta t = \pi \sqrt{\frac{r^3}{\mu}} \quad (42)$$

or $\Delta t = 4200$ s or about 70 minutes. This time may be used as a characteristic value for a time interval $[t_i, t_{i+1}]$. On the other hand, the velocity of the asteroid varies slowly over much larger time intervals – in the order of one year. Thus, considering that $\Delta t/(1\text{year})$ is in the order of 1×10^{-4} , the velocity v_a may be taken to have a constant value v_{ai} in a time interval $[t_i, t_{i+1}]$. This allows for the direct evaluation of the integral in (41). Integrating by parts, and noting that $\theta = -\theta_b$ at time $t = t_i$, and that $\theta = \theta_b$ at time t_{i+1} , this leads to

$$\Delta\zeta_i = -\kappa \frac{Gm_{ci}}{h} v_{ai} [(t_e - t_{i+1})) \sin \theta_b + (t_e - t_i)) \sin \theta_b] + \kappa \frac{Gm_{ci}}{h} v_{ai} \int_{t_i}^{t_{i+1}} \sin \theta dt \quad (43)$$

We note that

$$\int_{t_i}^{t_{i+1}} \sin \theta dt = 0 \quad (44)$$

because $\sin \theta$ is antisymmetric about the midpoint of the interval $[t_i, t_{i+1}]$. Next, simplifying (43) it follows that

$$\Delta\zeta_i = -\kappa v_{ai} \frac{Gm_{ci}}{h} (2t_e - (t_{i+1} + t_i)) \sin \theta_b \quad (45)$$

For the case $\dot{\theta} < 0$, the above procedure is repeated with the only difference that $|\dot{\theta}| = -\dot{\theta}$ and that $\theta = \theta_b$ at time $t = t_i$, and that $\theta = -\theta_b$ at time t_{i+1} . The result is again (45), i.e. the deflection caused by the motion in the time interval $[t_i, t_{i+1}]$ is independent of whether the spacecraft is moving clockwise or counter-clockwise.

A simpler form for $\Delta\zeta_i$ can be obtained by defining the time

$$\bar{t}_i = \frac{t_{i+1} + t_i}{2} \quad (46)$$

and noting that

$$\Delta\zeta_i = -\kappa v_{ai} (t_e - \bar{t}_i) \frac{2 \sin \theta_b Gm_{ci}}{h} \quad (47)$$

3.2.1 The impulse exerted and the average force

For a simplifying interpretation of (47) we next consider the impulse imparted to the asteroid by the gravitational force from the spacecraft during one pass of the spacecraft along the segment of the Keplerian orbit, i.e. during the time interval $[t_i, t_{i+1}]$. Note that due to the symmetry of the orbit segment about the x -axis in Figure 6, the impulse will only have an x -component, and may be written as

$$I_i = \int_{t_i}^{t_{i+1}} \frac{Gm_a m_{ci}}{r^2} \cos \theta dt \quad (48)$$

Using (39), (48) can be written as

$$I_i = \int_{t_i}^{t_{i+1}} \frac{Gm_a m_{ci}}{h} \cos \theta |\dot{\theta}| dt \quad (49)$$

or

$$I_i = \frac{2Gm_a m_{ci}}{h} \sin \theta_b . \quad (50)$$

Also, for later use, we note that the angular momentum can be written in terms of the periapsis distance r_p and the eccentricity e of the orbit, i.e. (cf. [22, 23])

$$h = \sqrt{\mu_a r_p (1 + e)} , \quad (51)$$

where $\mu_a = Gm_a$ is the gravitational parameter for the asteroid. This leads to the expression

$$I_i = \frac{2Gm_a m_c}{\sqrt{\mu_a r_p (1 + e)}} \sin \theta_b . \quad (52)$$

Next, using (50) it follows that (47) can be written in the form

$$\Delta \zeta_i = -\frac{\kappa}{m_a} (t_e - \bar{t}_i) I_i v_{ai} \quad (53)$$

and the total $\Delta \zeta$ is then obtained as

$$\Delta \zeta = -\frac{\kappa}{m_a} \sum_{i=1}^N (t_e - \bar{t}_i) I_i v_{ai} \quad (54)$$

Defining the average force that acts during the time interval $[t_i, t_{i+1}]$ by

$$\bar{F}_i = \frac{I_i}{\Delta t} \quad (55)$$

where

$$\Delta t = t_{i+1} - t_i \quad (56)$$

we may write $\Delta \zeta_i$ in the form

$$\Delta \zeta_i = -\frac{\kappa}{m_a} (t_e - \bar{t}_i) \bar{F}_i v_{ai} \Delta t \quad (57)$$

Now, using (57) in (37) the total deflection can be written as

$$\Delta \zeta = -\frac{\kappa}{m_a} \sum_{i=1}^N (t_e - \bar{t}_i) \bar{F}_i v_{ai} \Delta t \quad (58)$$

3.3 Comparison to deflection from a constant force: the stationary and displaced-orbit gravity tractors

The deflection that can be realized using a Keplerian gravity tractor may be compared to the corresponding deflections that would result from a stationary [12,15] or displaced-orbit [17] gravity tractors.

3.3.1 The stationary gravity tractor

For the stationary gravity tractor, referring to Figures 7, the corresponding force exerted on the asteroid by a spacecraft of mass (m_c) is

$$F_s = \frac{Gm_cm_a}{(\alpha r_a)^2} \quad (59)$$

where $\alpha > 1$ is a parameter that determines the distance to the spacecraft from the center of mass

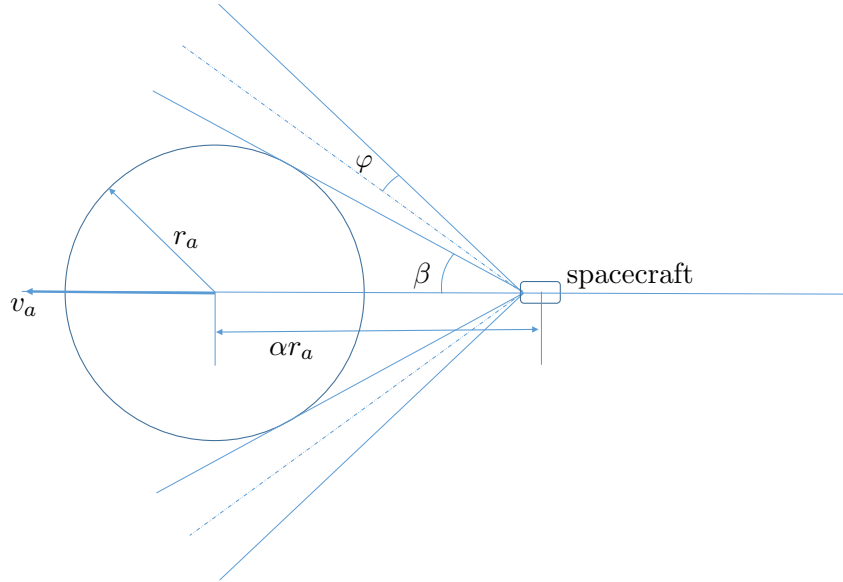


Figure 7: The stationary gravity tractor.

of the asteroid, and r_a is the radius of the asteroid, as before.

In this case, it follows from (38) that the contribution to the deflection $\Delta\zeta$ at the time of projected collision t_e from the constant gravitational force acting in the time interval $[t_i, t_{i+1}]$ can be calculated as

$$\Delta\zeta_i^c = -\kappa \int_{t_i}^{t_{i+1}} (t_e - t) v_{ai} \frac{Gm_c}{(\alpha r_a)^2} dt, \quad (60)$$

While the mass of the spacecraft will decrease slowly over time as it burns fuel to generate the required thrust, this change in mass may be neglected in the small time interval $[t_i, t_{i+1}]$. Thus denoting the mass of the spacecraft in that time interval by m_{ci} we have from (60) that

$$\Delta\zeta_i^c = \frac{\kappa}{2} \left[(t_e - t_{i+1})^2 - (t_e - t_i)^2 \right] v_{ai} \frac{Gm_{ci}}{(\alpha r_a)^2} \quad (61)$$

Expanding and simplifying the term within square brackets of the right hand side of (61) gives

$$\Delta\zeta_i^c = \frac{\kappa}{2} [2t_e(t_i - t_{i+1}) + t_{i+1}^2 - t_i^2] v_{ai} \frac{Gm_{ci}}{(\alpha r_a)^2} \quad (62)$$

or

$$\Delta\zeta_i^c = \frac{\kappa}{2} (t_{i+1} - t_i) [t_{i+1} + t_i - 2t_e] v_{ai} \frac{Gm_{ci}}{(\alpha r_a)^2} \quad (63)$$

Now using (46), (56), and (2), (63) may be written as

$$\Delta\zeta_i^c = -\frac{\kappa}{m_a} (t_e - \bar{t}_i) \Delta t v_{ai} F_s^i \quad (64)$$

where the force from the stationary gravity tractor in the i th time interval is

$$F_s^i = \frac{Gm_a m_{ci}}{(\alpha r_a)^2} \quad (65)$$

is the force on the asteroid from the stationary gravity tractor during the time interval $[t_i, t_{i+1}]$.

3.3.2 The displaced-orbit gravity tractor

The displaced-orbit gravity tractor is shown schematically in Figure 8. The net perturbing gravi-

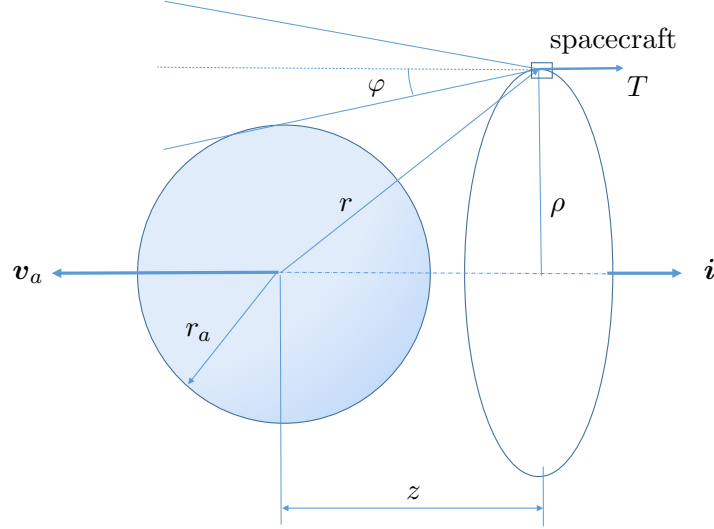


Figure 8: The displaced-orbit gravity tractor.

tational force that acts on the asteroid from the spacecraft is (cf. [17])

$$\mathbf{F}_d = \frac{Gm_a m_c}{r^2} \frac{z}{r} \mathbf{i} \quad (66)$$

and acts in a direction opposite to the velocity. The corresponding required thrust on the spacecraft that keeps it in its orbital plane with respect to the asteroid is

$$T = F_d = \frac{Gm_a m_c}{r^2} \frac{z}{r} \quad (67)$$

It further follows from Figure 8 that

$$r = \sqrt{\rho^2 + z^2} \quad (68)$$

and that

$$\rho = r_a + z \tan \beta \quad (69)$$

or

$$r = \sqrt{(r_a + z \tan \varphi)^2 + z^2} \quad (70)$$

It is described [17] that the largest perturbing gravitational force that can be exerted on the asteroid by the spacecraft while satisfying the non-impingement conditions for $\varphi = 20^\circ$ occurs for $z = 2.1r_a$. Using (70) and (66) this implies

$$F_d = 0.21 \frac{Gm_a m_c}{r_a^2} . \quad (71)$$

The force F_d will slowly decrease as m_c decreases. However, in the small time interval $[t_i, t_{i+1}]$ it may be assumed constant, corresponding to the mass of the spacecraft in that time interval. Thus for the force in the i th time interval we have

$$F_d^i = 0.21 \frac{Gm_a m_{ci}}{r_a^2} . \quad (72)$$

As in the case of the stationary gravity tractor, the contribution to the deflection at time t_e from the action of F_d^i in the time interval $[t_i, t_{i+1}]$ may be written as

$$\Delta \zeta_i^d = -\frac{\kappa}{m_a} (t_e - \bar{t}_i) \Delta t v_{ai} F_d^i \quad (73)$$

The contributions to the deflection from a Keplerian gravity tractor, the stationary gravity tractor, and the displaced orbit gravity tractor from action during a time interval $[t_i, t_{i+1}]$ have identical expressions save for the magnitudes of the forces (average force in the case of the Keplerian gravity tractor) for a given mass of the spacecraft m_{ci} . A measure of their relative efficiency may therefore be obtained by a direct comparison of the forces. This comparison will be made in Section 4.

3.4 An expression for the total deflection

Finally in this section we derive an expression for the total deflection of the asteroid in terms of the mass of the spacecraft and the amount of fuel burned. This expression will be obtained by directly evaluating (58).

Using the definition of Δt in (56) we note that

$$t_i = t_s + (i - 1)\Delta t \quad (74)$$

$$t_{i+1} = t_s + i\Delta t \quad (75)$$

Next, substituting (74) and (75) in (46) it follows that

$$\bar{t}_i = t_s + i\Delta t - \frac{\Delta t}{2} \quad (76)$$

The mass of the spacecraft will decrease every time the thruster is fired to change the direction of the velocity at the times $t_i : i = 1 \dots N$. The amount of fuel mass that is burned is itself dependent upon the current mass of the spacecraft. This mass of fuel burned at time t_i may be written as (cf. [28])

$$\Delta m_i = m_{ci}(1 - e^{-\frac{\Delta v}{I_{sp}g_0}}) \quad (77)$$

where m_{ci} is the mass of the spacecraft at time t_i , I_{sp} is the specific impulse of the spacecraft's thruster, Δv is the change in velocity required, and $g_0 = 9.81 \text{ m/s}^2$ is the acceleration due to gravity at the surface of Earth.

Thus for the mass of the spacecraft itself we have

$$m_{c(i+1)} - m_{ci} = -\Delta m_i = -m_{ci}(1 - e^{-\frac{\Delta v}{I_{sp}g_0}}) \quad (78)$$

or

$$m_{c(i+1)} = m_{ci}e^{-\frac{\Delta v}{I_{sp}g_0}}. \quad (79)$$

Denoting the initial mass of the spacecraft by m_{c1} this leads to

$$m_{ci} = m_{c1}e^{-\frac{\Delta v}{I_{sp}g_0}(i-1)} \quad (80)$$

Now using (80) in (50), it follows from (55) that

$$\bar{F}_i = \frac{2Gm_a \sin \theta_b}{h\Delta t} m_{c1}e^{-\frac{\Delta v}{I_{sp}g_0}(i-1)} \quad (81)$$

or

$$\bar{F}_i = \lambda m_{c1}e^{-\frac{\Delta v}{I_{sp}g_0}(i-1)} \quad (82)$$

where we have defined the constant λ for brevity such that

$$\lambda = \frac{2Gm_a \sin \theta_b}{h\Delta t} \quad (83)$$

Substituting (82) in (57) and using (76) we have

$$\Delta \zeta_i = -\frac{\kappa}{m_a}(t_e - t_s - i\Delta t - \frac{\Delta t}{2})\lambda v_{ai}m_{c1}e^{-\frac{\Delta v}{I_{sp}g_0}(i-1)}\Delta t \quad (84)$$

or

$$\Delta \zeta_i = -\frac{\kappa}{m_a}(t_e - t_s - \frac{\Delta t}{2})\lambda v_{ai}m_{c1}e^{-\frac{\Delta v}{I_{sp}g_0}(i-1)}\Delta t + \frac{\kappa}{m_a}\Delta t^2 i\lambda v_{ai}m_{c1}e^{-\frac{\Delta v}{I_{sp}g_0}(i-1)} \quad (85)$$

As has already been discussed, the time interval Δt for one pass of the spacecraft on the orbit segment is small in relation to the time interval $t_e - t_s$, i.e. how long before the projected collision the gravity tractor action starts. We can therefore neglect the term $\frac{\Delta t}{2}$ in the expression $(t_e - t_s - \frac{\Delta t}{2})$ in (85). Now using (37) we have

$$\Delta \zeta = -\frac{\kappa}{m_a}(t_e - t_s)\lambda m_{c1}\Delta t \sum_{i=1}^N v_{ai}e^{-\frac{\Delta v}{I_{sp}g_0}(i-1)} + \frac{\kappa}{m_a}\Delta t^2 \lambda m_{c1} \sum_{i=1}^N v_{ai}ie^{-\frac{\Delta v}{I_{sp}g_0}(i-1)} \quad (86)$$

Further evaluation (86) requires taking into account the slowly varying velocity v_a , unless the asteroid is on a circular orbit when v_{ai} will be constant. In that case, denoting the constant velocity of the asteroid by v_a and defining

$$q = \frac{\Delta v}{I_{sp} g_0} \quad (87)$$

for brevity, the sums in (86) may be evaluated to give (see for example [21])

$$\Delta \zeta = -\frac{\kappa}{m_a} \lambda v_a m_{c1} \left((t_e - t_s) \Delta t \frac{e^{q-Nq}(e^{Nq} - 1)}{e^q - 1} - \Delta t^2 \frac{e^{q-Nq}(e^{q+Nq} + N - e^q(1 + N))}{(e^q - 1)^2} \right) \quad (88)$$

An example of the evaluation of (86) on an elliptic orbit, i.e. where the velocity of the asteroid shows large variations, will be discussed in Section 6.

4 Design of the orbit segment: maximizing the average force

As follows from (58) maximizing the average force that is exerted on the asteroid in each time interval $[t_i, t_{i+1}]$ corresponds to the largest possible $\Delta \zeta$ that can be obtained, with all other variables fixed. In what follows, we will consider the various types of Keplerian orbits that the spacecraft may move along, and how the average force depends on their characteristics. The aim is to choose these characteristics so that the average force, and therefore the final deflection, are as large as possible. The attainable average forces will be compared to the constant forces that can be obtained from the stationary gravity tractor and the displaced-orbit gravity tractor.

4.1 Conditions for avoiding plume impingement

It may be noted that based on (50) alone, the overall impulse from one pass of the spacecraft on the orbit segment will be largest if h is chosen as small as possible and if $\theta_b = \frac{\pi}{2}$. Using (53) this would also result in the largest possible contribution to the deflection from that time interval. However, the need to avoid impingement of the thruster plume on the asteroid will modify the problem. Thus in this section we consider the problem of avoiding plume impingement during restricted Keplerian motion. The problem is analogous to the consideration of the exhaust plume that is done for the stationary gravity tractor in [12].

Figure 9 shows a situation with a spacecraft firing its thruster to generate a force F . The plume half angle is denoted as φ , and γ is the flight path angle at that point on the orbit segment given by (cf. [22])

$$\gamma = \tan^{-1} \left(\frac{e \sin \theta_b}{1 + e \cos \theta_b} \right). \quad (89)$$

It is clear that plume impingement can be avoided by choosing a sufficiently large value for $r(\theta_b)$. Noting that $r(\theta_b)$ depends on the periapsis distance r_p , the eccentricity e , and the value of θ_b , a condition to avoid plume impingement can be derived as follows.

Referring to Figure 9 we note that

$$r_a = r(\theta_b) \cos(\varphi - \gamma), \quad (90)$$

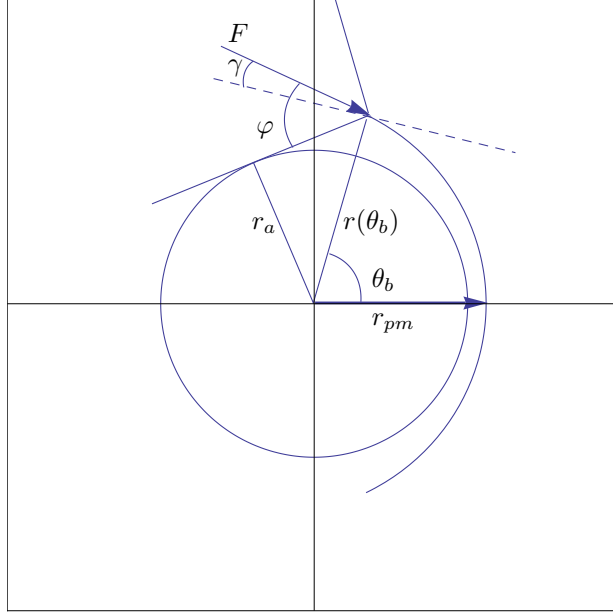


Figure 9: Effect of plume angle on minimum periapsis radius.

where r_a is the radius of the asteroid (or in the case of a non-spherical asteroid, the largest distance on the asteroid from the center of mass in the plane of motion of the spacecraft). An expression for $r(\theta_b)$ can be found from the equation of path for the two-body problem (cf. [22, 23])

$$r(\theta) = \frac{r_p(1+e)}{1+e\cos\theta}, \quad (91)$$

with $\theta = \theta_b$. Denoting the smallest allowable value of r_p by r_{pm} and using (91) and (90), it follows that

$$r_{pm} = \frac{(1+e\cos\theta_b)}{(1+e)\cos(\varphi-\gamma)} r_a. \quad (92)$$

Thus (92) allows us to determine how close a given orbit segment can come to the asteroid without violating the plume non-impingement condition. This in turn determines the maximum average force that can be obtained from the orbit segment as will be seen in the following sections.

4.2 Restricted motion along a circular orbit

The simplest orbit segment that can be used to impart an impulse to the asteroid per the discussion above is one that is circular. In this case, r_{pm} is independent of θ_b as follows from (92) by using $e = 0$ and $\gamma = 0$. The resulting value

$$r_{pm} = \frac{r_a}{\cos\varphi}. \quad (93)$$

is simply the radius of the smallest circle that satisfies the non-impingement condition.

For a given value of the bounding angle θ_b the time of flight between points A and B on a circular orbit of radius r is (cf. [24, 25])

$$\Delta t = 2\theta_b \sqrt{\frac{r^3}{\mu}}. \quad (94)$$

Thus considering a single pass on such an orbit segment with bounding angle θ_b and using (52) with $e = 0$ and $r_p = r$, the net impulse that is imparted to the asteroid per unit time (or average force as defined in (55)) can be calculated as

$$\bar{F}_i = \frac{I_i}{\Delta t} = \frac{Gm_{ci}m_a \sin \theta_b}{\theta_b r^2}, \quad (95)$$

where as before m_{ci} is the mass of the spacecraft during the corresponding time interval $[t_i, t_{i+1}]$. Using (93) to find the smallest allowable radius in order to maximize the average force

$$\bar{F}_{i(\max)} = \frac{Gm_{ci}m_a \sin \theta_b \cos^2 \varphi}{r_a^2 \theta_b}. \quad (96)$$

For the sake of comparison with the stationary and displaced-orbit gravity tractors, we define the nondimensional maximum average force (for given values of the plume angle φ and the bounding angle θ_b).

$$\eta_k(\theta_b, \varphi) = \frac{\sin \theta_b \cos^2 \varphi}{\theta_b}, \quad (97)$$

by scaling (96) by $\frac{Gm_{ci}m_a}{r_a^2}$.

4.2.1 Comparison of the deflecting forces

The nondimensional force for the stationary gravity tractor can be defined the same way as in (97) and based on (65):

$$\eta_s = \frac{1}{\alpha^2}. \quad (98)$$

The value for α in for example [12, 15] is $\alpha = 1.5$. It has been shown, however, (see [26]) that this value (and small values of α in general) may lead to oscillations of the altitude of the hovering spacecraft with respect to the asteroid. Therefore, as in [17], we also consider $\alpha = 2.5$ as a more realistic value for comparisons below. Overall, it may be noted that a small α leads to a large cant angle and therefore inefficiency with respect to thrust developed by the spacecraft. Similarly a large α means a smaller force between the asteroid and the spacecraft lowering the overall impulse imparted.

Lastly for the nondimensional force from the displaced-orbit gravity tractor we have

$$\eta_d = 0.21 \quad (99)$$

which follows by scaling (72) by $\frac{Gm_{ci}m_a}{r_a^2}$.

Figure 10 shows the nondimensional average forces that are exerted by the Keplerian (circular orbit), stationary, and displaced-orbit gravity tractors. The average force from the Keplerian gravity tractor depends on the value of the bounding angle θ_b and is plotted as a function of θ_b . The plume

half angle which also affects the net force from the Keplerian gravity tractor is here set to $\varphi = 20^\circ$ for the sake of numerical comparison. The average force from the stationary and displaced-orbit gravity tractors do not depend on θ_b and are therefore shown as constant values. It follows that for an appropriately chosen bounding angle, i.e. $\theta_b < 1.9$ rad the Keplerian gravity tractor will exert the largest net force on the asteroid.

Overall, the average force from the Keplerian gravity tractor is large because of the closeness of the spacecraft to the asteroid that can be achieved. The average force is especially large for small values of θ_b (as the orbit segments remain close to periapsis). However, there will be limits on how small θ_b can be made in practice. For example, when the burn times required to effect the required changes in velocity of the spacecraft are not much smaller than the time between burns, the present analysis is not strictly valid. A general discussion of the time between burns is presented in Section 4.4

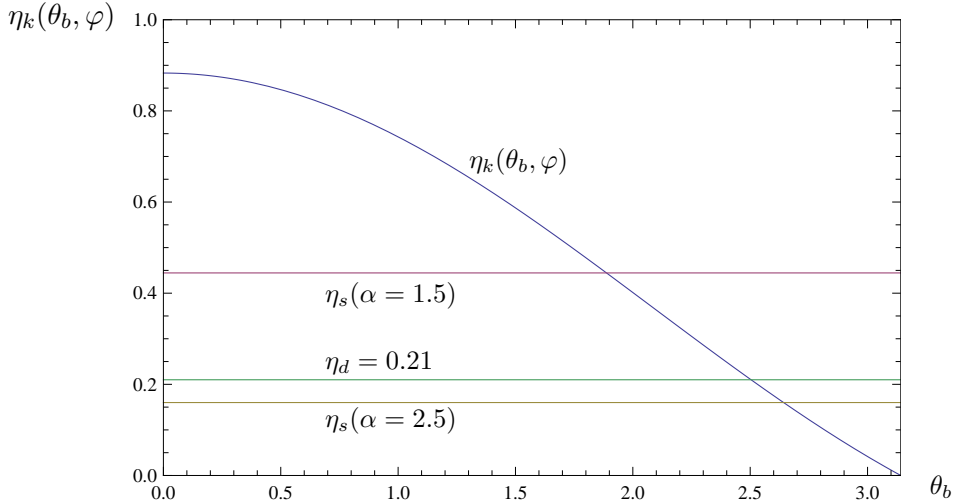


Figure 10: A comparison of the average force exerted by the stationary, displaced-orbit, and Keplerian gravity tractor in a circular orbit ($\varphi = 20^\circ$).

4.3 Restricted motion along non-circular orbits

The time of flight (TOF) between the angles $\theta = -\theta_b$ and $\theta = \theta_b$ on an orbit of eccentricity e and periapsis distance r_p is determined as (see for example [24, 25])

$$\Delta t_e = 2\sqrt{\frac{r_p^3}{\mu_a(1-e)^3}}(E_b - e \sin E_b) \quad e < 1 \quad (\text{ellipse}), \quad (100)$$

$$\Delta t_h = 2\sqrt{\frac{-r_p^3}{\mu_a(1-e)^3}}(F_b - e \sin F_b) \quad e > 1 \quad (\text{hyperbola}), \quad (101)$$

$$\Delta t_p = \left(\frac{(2r_p)^{3/2}}{\sqrt{\mu_a}}\right)\left(\frac{1}{3}\tan\frac{\theta_b^3}{2} + \tan\frac{\theta_b}{2}\right) \quad e = 1 \quad (\text{parabola}), \quad (102)$$

where E_b is the eccentric anomaly determined by

$$\cos E_b = \frac{e + \cos \theta_b}{1 + e \cos \theta_b} \quad (e < 1), \quad (103)$$

and F_b is the hyperbolic anomaly determined by

$$\cosh F_b = \frac{e + \cos \theta_b}{1 + e \cos \theta_b} \quad (e > 1). \quad (104)$$

Thus using (52) the impulse imparted per unit time (or average force) for the elliptic orbit can be written as

$$\frac{I_i}{\Delta t_e} = \frac{Gm_a m_{ci}}{r_p^2} \sqrt{\frac{(1-e)^3}{1+e}} \frac{\sin \theta_b}{E_b - e \sin E_b}, \quad (105)$$

and for the parabolic orbit

$$\frac{I_i}{\Delta t_p} = \frac{Gm_a m_{ci}}{4r_p^2} \left(\frac{1}{3} \tan^3 \frac{\theta_b}{2} + \tan \frac{\theta_b}{2} \right). \quad (106)$$

Similarly, for the hyperbolic orbit, it is obtained that

$$\frac{I_i}{\Delta t_h} = \frac{Gm_a m_{ci}}{r_p^2} \sqrt{\frac{(e-1)^3}{1+e}} \frac{\sin \theta_b}{e \sin F_b - F_b}. \quad (107)$$

In each case, the largest impulse per time is obtained if r_p is chosen as $r_{pm}(\theta_b)$ given by (92). Thus, using (92) in (105)-(107) and scaling each average force by $\frac{Gm_a m_{ci}}{r_a^2}$ we define the nondimensional average force $\eta(\theta_b, \varphi, e)$ through

$$\eta(\theta_b, \varphi, e) = \begin{cases} \frac{1}{A(\theta_b, \varphi, e)} \sqrt{\frac{(1-e)^3}{1+e}} \frac{\sin \theta_b}{E_b - e \sin E_b} & (e < 1), \\ \frac{1}{4A(\theta_b, \varphi, e)} \left(\frac{1}{3} \tan^3 \frac{\theta_b}{2} + \tan \frac{\theta_b}{2} \right) & (e = 1), \\ \frac{1}{A(\theta_b, \varphi, e)} \sqrt{\frac{(1-e)^3}{1+e}} \sqrt{\frac{(e-1)^3}{1+e}} \frac{\sin \theta_b}{e \sin F_b - F_b} & (e > 1), \end{cases} \quad (108)$$

where, using (92), we have defined

$$A(\theta_b, \varphi, e) = \frac{(1 + e \cos \theta_b)^2}{(1 + e)^2 \cos^2(\varphi - \gamma)} \quad (109)$$

for brevity.

Thus, as in the case of the circular orbit, the average force exerted on the asteroid can be studied as a function of θ_b , now with the eccentricity e acting as a parameter modifying the orbit. Figure 11 shows plots of $\eta_k(\theta_b, \varphi, e)$ with respect to θ_b and for various values of the eccentricity e . The value of φ used is again 20° . For comparison, the earlier derived corresponding values of η_s and η_d are also shown. We conclude from Figure 11 that even though according to (40) alone, the best solution would have been to always choose $e = 0$, the plume non-impingement condition means that there are values of θ_b for which a larger average force can be obtained with $e \neq 0$. The overall

largest values of η_k are obtained for small values of θ_b and large values of the eccentricity. It should be noted, however, that these cases may be difficult to realize in practice due to the corresponding short times between impulsive thrusts. In addition, as in the case of the circular orbit we note that when the flight times approach the thrust durations necessary to affect the required Δv 's the assumption of instantaneous impulsive thrust will not be satisfied and further analysis would be necessary. This will be further discussed in the next section.

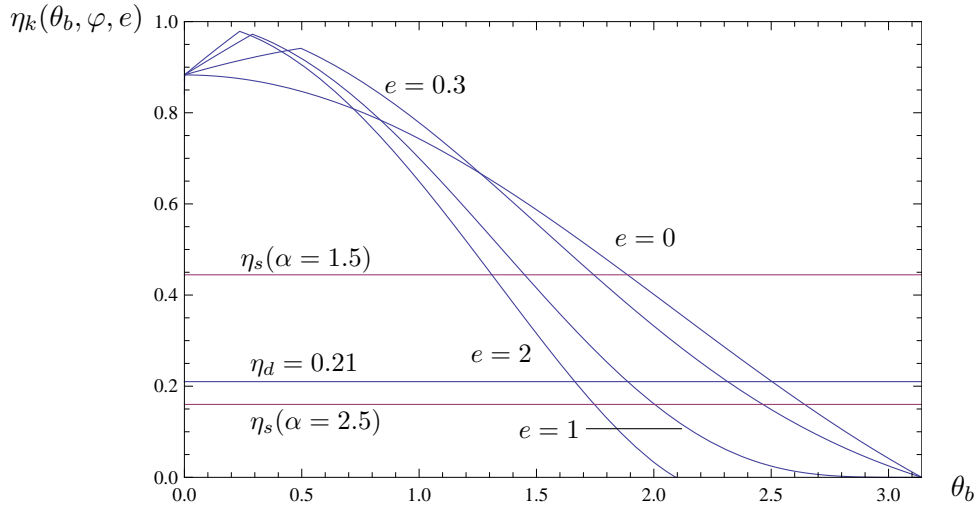


Figure 11: A comparison of the average force exerted by the Keplerian gravity tractor on orbits of various eccentricities. The corresponding forces from the stationary gravity tractor and the displaced-orbit gravity tractor are also shown for comparison. The plume angle is $\varphi = 20^\circ$.

4.4 The time between impulsive thrusts

As is common in the preliminary analysis of impulsive velocity changes (Δv 's), we have above assumed that the impulsive thrusts that change the direction of the velocity of the spacecraft moving along a Keplerian orbit segment, are applied instantaneously. In practice, of course, the implication is only that the duration of the thrusts is small compared to a characteristic time of flight on the orbit. For this reason, it is important to consider the time of flight on the Keplerian orbit segment and verify that it is much larger than the duration of a typical thrust.

The time between the impulsive thrusts, i.e. between the angles $-\theta_b$ and θ_b , or vice-versa, can be obtained directly from (100)-(102), where r_p is set to r_{pm} using (92). The resulting times of flight are shown in Figure 12. Canonical time units for the asteroid are used such that (cf. [27])

$$1 \text{ TU} = \sqrt{\frac{r_a^3}{\mu_a}}. \quad (110)$$

To get a sense of the length of 1 TU, consider as before an asteroid of diameter 100 m and mass 8.4×10^9 kg. Then, it follows that $1 \text{ TU} \approx 1340 \text{ s} = 22 \text{ min}$. Therefore, for example, near the value of $\theta_b = 1.5$ rad where, for small eccentricities, $\eta_k(\theta_b, \varphi, e) \approx 0.6$ (see Figure 11) the time between impulsive thrusts is in the order of 3 TU or 66 minutes.

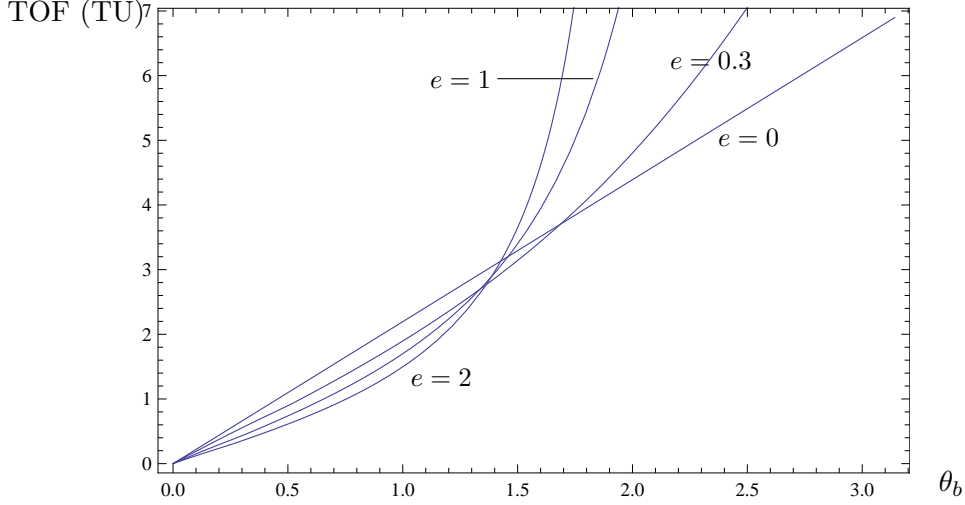


Figure 12: Times between impulsive thrusts as a function of θ_b on the orbit segments for various eccentricities; $\varphi = 20^\circ$.

One implication of the time between impulsive thrusts is that the actual duration of the thrusts themselves must be much smaller than the time between the thrusts. In the next section, we derive an expression for the required Δv 's and estimate the corresponding thrust times in order to verify that the assumption of impulsive thrusts is valid.

4.5 The impulsive velocity change

In order to change the direction of the velocity of the spacecraft on the orbit segment, the required Δv is exactly twice the magnitude of the velocity. The velocity at the bounding angles can be obtained from the expression for the (specific) energy of the orbit (cf. [22, 23])

$$\mathcal{E} = \frac{v^2}{2} - \frac{\mu_a}{r} = -\frac{\mu_a}{2a}, \quad (111)$$

where a is the semimajor axis of the orbit. Noting that the semimajor axis can be written as (cf. [22, 23])

$$a = \frac{r_p}{1 - e}, \quad (112)$$

and using the equation of path (91), it follows that the velocity magnitude at the bounding angles is

$$v_m = \sqrt{\frac{\mu_a}{r_p(1 + e)}} \sqrt{1 + e^2 + 2e \cos \theta_b}. \quad (113)$$

Then, the Δv on the orbit with $r_p = r_{pm}$ is

$$\Delta v = 2 \sqrt{\frac{\mu_a}{r_{pm}(1 + e)}} \sqrt{1 + e^2 + 2e \cos \theta_b}, \quad (114)$$

or using (92) in (114)

$$\Delta v = 2\sqrt{\frac{\mu_a}{r_a}} \sqrt{\frac{\cos(\varphi - \gamma)}{1 + e \cos \theta_b}} \sqrt{1 + e^2 + 2e \cos \theta_b} . \quad (115)$$

We note that the expression for Δv in (115) is in the form

$$\Delta v = \sqrt{\frac{\mu_a}{r_a}} \nu(\theta_b, e, \varphi) , \quad (116)$$

where we have defined

$$\nu(\theta_b, e, \varphi) = 2\sqrt{\frac{\cos(\varphi - \gamma)}{1 + e \cos \theta_b}} \sqrt{1 + e^2 + 2e \cos \theta_b} . \quad (117)$$

and $\sqrt{\frac{\mu_a}{r_a}}$ is the circular satellite velocity at a radius of r_a around the asteroid.

Figure 13 shows the dependence of $\nu(\theta_b, e, \varphi)$ on θ_b and e . The value of $\varphi = 20^\circ$ has been used for the sake of example. Thus for an orbit of given eccentricity, the required Δv will be smallest

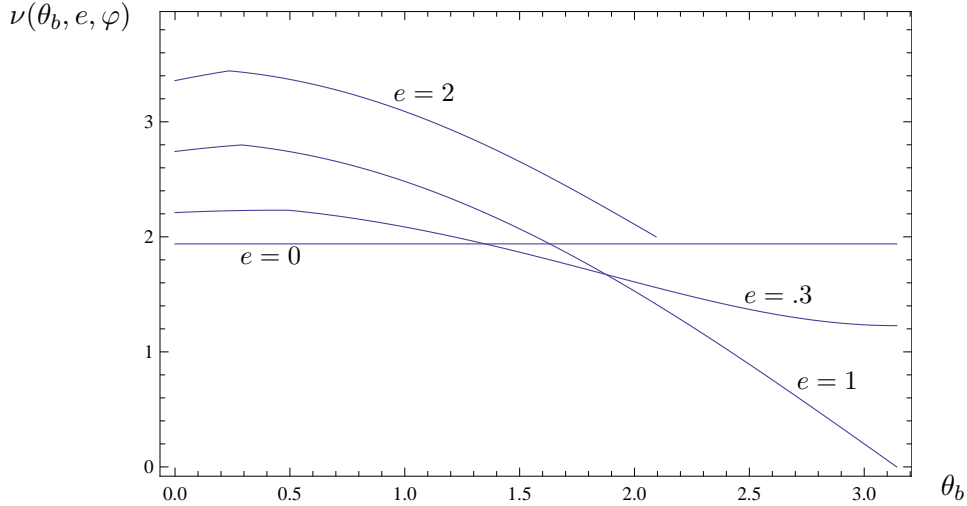


Figure 13: Nondimensional impulsive Δv 's as functions of the bounding angle θ_b for various values of e ; $\varphi = 20^\circ$.

for large bounding angles as the velocity will decrease with increasing true anomaly. The required Δv generally increases with decreasing bounding angle. However, for small values of the bounding angle and a given eccentricity, it is seen that there is a region where the required Δv decreases with the bounding angle θ_b . This is due to the fact that for these values of θ_b the spacecraft is generally close to the surface of the asteroid and the plume impingement constraint is active. Consequently, as θ_b decreases, the minimum periapsis distance is required to increase leading to a smaller velocity v_b and therefore a smaller Δv .

The values of the required Δv 's have implications on the choice of thrusters for the spacecraft. As an example we consider an asteroid of mass 8.4×10^9 kg and radius 100 m (as before). The Δv that would be required on a circular orbit segment (with $\varphi = 20^\circ$) is 0.145 m/s. Now, the impulsive

thrust F required to obtain a given Δv for the spacecraft can be found from the relation

$$T\Delta t = m_c \Delta v . \quad (118)$$

where Δt is the duration of the thrust. If we assume, for the sake of example, a spacecraft of mass 2000 kg, the impulse required is 290 N-s which could for example be obtained by a 1-N force acting over 290 seconds. The duration of 290 s can be compared to the time of flight of 4600 s (that is obtained using (94) with r_p set to r_m from (93)) thus justifying the model of impulsive velocity changes.

4.6 Full orbits between impulsive thrusts

Depending on the configuration of the thrusters on a spacecraft, the spacecraft may need some minimum amount of time in order to re-orient itself between successive firings of the thrusters, i.e. so that the thrusters are pointing in a desired direction. In the case of circular and elliptic orbits, a technique to increase the time between impulsive thrusts, if necessary, may be for the spacecraft to complete one or more full orbits around the asteroid between the bounding angles where the impulsive thrusts are executed. For example, referring to Figure 6 the spacecraft could start at point A , move past point B without an impulsive thrust at that point, and return to point B after a full cycle on the orbit, at which time an impulsive thrust could change the direction of motion sending the spacecraft back to A in a clockwise direction. In this way, while the impulsive thrusts required at A and B remain unchanged, as well as the net impulse on the asteroid, the time between the impulsive thrusts can be increased.

Figure 14 shows the average force for the case of an added orbit period, as a function of the bounding angles, for three values of the eccentricity. For comparison, the average force from the stationary gravity tractor with $\alpha = 2.5$ is also shown.

Overall, as would be expected, the impulse per time is smaller for all angles of θ_b in comparison to the case of no extra orbit cycles. This decrease is especially large for small values of θ_b . However, this approach can still give a larger average force than the stationary gravity tractor with $\alpha = 2.5$.

5 Impulse imparted per mass of fuel used

The contribution to the total deflection at the time of encounter t_e from an impulse imparted to the asteroid at time t_i is given in (53). Thus $\Delta\zeta_i$ in (53) is proportional to the impulse I_i . Therefore a consideration of impulse imparted I_i per amount of fuel burned in the spacecraft during that same time interval gives another measure of the efficiency of the different asteroid deflection methods. In this section we derive expressions for the impulse imparted per mass of fuel burned and compare them between the Keplerian, stationary, and displaced-orbit gravity tractors.

The mass of fuel burned during an impulsive velocity change when the spacecraft mass is m_{ci} is given in (77). On the other hand, an expression for the impulse imparted to the asteroid from one pass of the spacecraft on a Keplerian orbit segment is given in (52). Noting that an impulsive thrust takes place at the beginning of each pass on a Keplerian orbit segment, the impulse imparted during a time interval $[t_i, t_{i+1}]$ per mass of fuel burned at the beginning of the interval can be expressed as

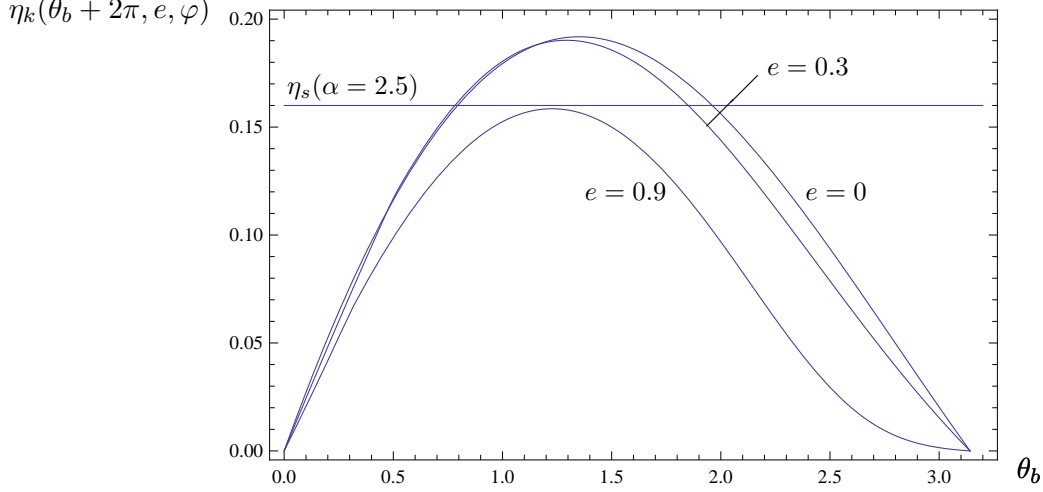


Figure 14: Impulse per time imparted by elliptic orbits with one extra orbit cycle; $\varphi = 20^\circ$

$$\frac{I_i}{\Delta m_i} = \frac{2Gm_a \sin \theta_b}{\sqrt{\mu_a r_p (1+e)(1-e^{-\frac{\Delta v}{I_{sp}g_0}})}}. \quad (119)$$

This quantity will be referred to below as the *mass efficiency*.

Recall that a typical value for a Δv is in the order of 0.1 m/s per the discussion just before (118). At the same time, I_{sp} values realizable with current technology may range from hundreds of seconds for chemical rockets to several 1000 seconds for ion engines ([28]). Therefore it is clear that $I_{sp}g_0 \gg \Delta v$ and the ratio $\frac{\Delta v}{I_{sp}g_0}$ in (119) is generally small. Using (114) useful approximation for the mass efficiency can therefore be obtained from (119) in the form

$$\frac{I_i}{\Delta m_i} \approx \frac{I_{sp}g_0 \sin \theta_b}{\sqrt{1+e^2+2e \cos \theta_b}}, \quad (120)$$

meaning that it does not depend on the value of r_p . For easy comparisons below, we define the nondimensional mass efficiency by scaling the right hand side of (120) by $I_{sp}g_0$ so that

$$\zeta_k(\theta_b, e) = \frac{\sin \theta_b}{\sqrt{1+e^2+2e \cos \theta_b}}, \quad (121)$$

The corresponding mass efficiency for the stationary gravity tractor can be found by using (59) and the free body diagram for the spacecraft in Figure 15 to obtain a relation for the required thrust, which leads to

$$F_s = 2T \cos(\beta + \theta) = \frac{Gm_a m_c}{\alpha^2 r_a^2}. \quad (122)$$

On the other hand, with respect to fuel expenditure, the thrust required may be written in terms of the specific impulse and the rate of change of mass through (cf. [28])

$$T = I_{sp} \frac{dm'}{dt} g_0. \quad (123)$$

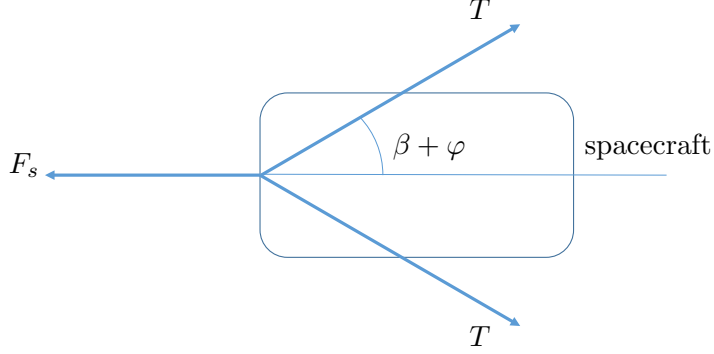


Figure 15: Free body diagram for the stationary gravity tractor.

where dm' is an infinitesimal mass expended in *one* of the thrusters in an infinitesimal time interval dt . Thus the impulse imparted in a time interval dt per mass of total fuel expended during that time becomes (noting that $2dm' = dm$, i.e. the change in mass of the spacecraft is twice the change in mass in each thruster)

$$\frac{dI}{dm} = \frac{F_s dt}{2dm'} , \quad (124)$$

or using (122) and (123)

$$\frac{dI}{dm} = I_{sp} g_0 \cos(\beta + \theta) ; , \quad (125)$$

indicating that the mass efficiency for the stationary gravity tractor is constant and only depends on the specific impulse. Scaling (125) by $I_{sp} g_0$ for a nondimensional mass efficiency we obtain

$$\zeta_s = \cos(\beta + \varphi) , \quad (126)$$

to be compared to $\zeta_k(\theta_b, e)$.

In the case of the displaced-orbit approach (see [17]), provided that the condition is met for plume non-impingement, the force that is acting on the asteroid is equal to the force that is developed by the thruster, as follows from (67). Therefore

$$\frac{dI}{dm} = \frac{F_d dt}{dm} = \frac{T dt}{dm} \quad (127)$$

or using (123) and noting that here $dm = dm'$

$$\frac{dI}{dm} = I_{sp} g_0 \quad (128)$$

The corresponding nondimensional mass efficiency is therefore $\zeta_d = 1$.

Figure 16 shows $\zeta_k(\theta_b, e)$ as a function of the bounding angle θ_b for various values of the eccentricity e . For the sake of comparison ζ_s (for the values of $\alpha = 1.5$ and $\alpha = 2.5$) are shown the same diagram. The values of β (see Figure 7) used for the stationary gravity tractor corresponding to $\alpha = 1.5$ and $\alpha = 2.5$ and are found from

$$\beta = \sin^{-1} \left(\frac{1}{\alpha} \right) , \quad (129)$$

which yields $\beta = 41.8^\circ$ and $\beta = 23.6^\circ$, respectively. In all cases, the plume angle is taken to be $\varphi = 20^\circ$ as before.

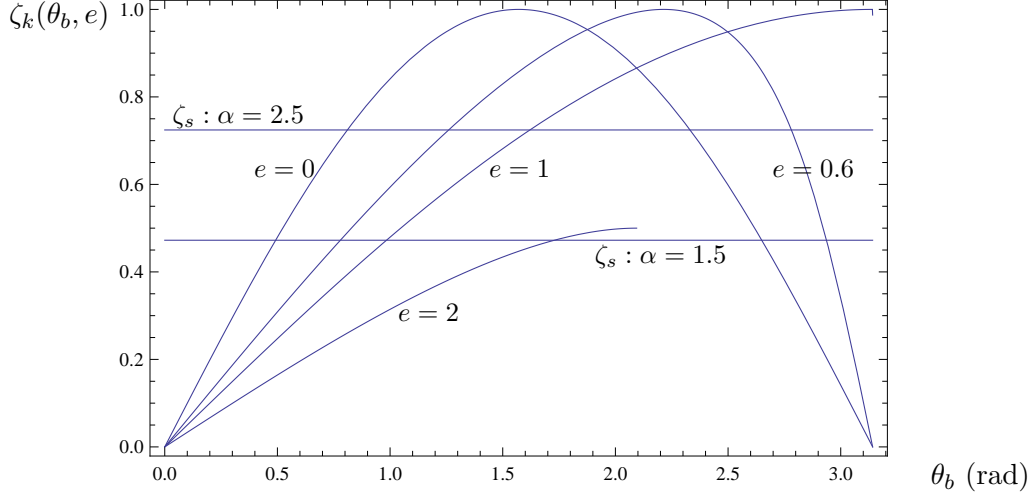


Figure 16: Comparison of impulse imparted per mass of fuel burned for the stationary and Keplerian gravity tractors.

Thus, for example, if one chooses $\theta_b = 2.2$ rad and $e = 0.6$ the nondimensional mass efficiency for the Keplerian gravity tractor is unity. At the same time, note that for the stationary gravity tractor the mass efficiency $\zeta_s = 0.72$ (for $\alpha = 2.5$) meaning that the Keplerian gravity tractor has a 40% higher mass efficiency in this case. Similarly, for the case $\alpha = 1.5$ ($\zeta_s = 0.47$), the Keplerian gravity tractor has a mass efficiency that is twice as large as for the stationary gravity tractor.

Lastly, we note that adding full cycles of elliptic orbits between the bounding angles $\pm\theta_b$, as detailed in Section 3.4, does not change the fuel requirements as the velocities at the points of impulsive thrusts remain the same.

6 Numerical Example

In Section 4 we compared the average forces from the stationary, displaced-orbit, and Keplerian gravity tractors. Using (57) and (64) this allows for a direct comparison of the contribution to the deflection caused by these gravity tractors from action during a small time interval $[t_i, t_{i+1}]$. In this section we consider a more complete comparison of the Keplerian and stationary gravity tractors by considering the total deflection caused by two similar spacecraft deployed as stationary and Keplerian gravity tractors.

6.1 An asteroid in an elliptic orbit: 2007 VK184

As an example we consider the hypothetical deflection of asteroid 2007 VK184 that is projected to have a close encounter with Earth in June 2048, but with no risk of a collision. The orbital elements of the asteroid are given in Table 1, [29]. In addition, the mass and radius of the asteroid are $m_a = 3.3 \times 10^9$ kg, and $r_a = 65$ m, respectively, [30].

Table 1: Orbital parameters for asteroid 2007 VK184

Epoch	JD 2457600.5 (2016-07-31)
Semimajor axis	1.7262 AU
Eccentricity	0.5697
Mean Anomaly	325.9 $^{\circ}$
Inclination	1.2209 $^{\circ}$
Longitude of ascending node	253.64 $^{\circ}$
Argument of perihelion	73.58 $^{\circ}$

For our purposes of comparing the efficiencies of the Keplerian and stationary gravity tractors, we will neglect the small inclination of the asteroid's orbit. Denoting the longitude of the ascending node by Ω and the argument of periapsis by ω , the longitude of perihelion Π may then be written as (cf. [31])

$$\Pi = \Omega + \omega \quad (130)$$

or $\Pi = 327.2^{\circ}$. Based on these assumptions, the orbits of the asteroid and that of Earth may be depicted as in Figure 17 where Earth's orbit is taken to be circular (see also [15]). The angle σ in the figure is

$$\sigma = 2\pi - \Pi \quad (131)$$

and has the value of $\sigma = 0.572$ rad, and the position of the projected encounter is shown by the vector \mathbf{r}_p . Denoting the true anomaly on the asteroid's orbit at the time of encounter by f_e we

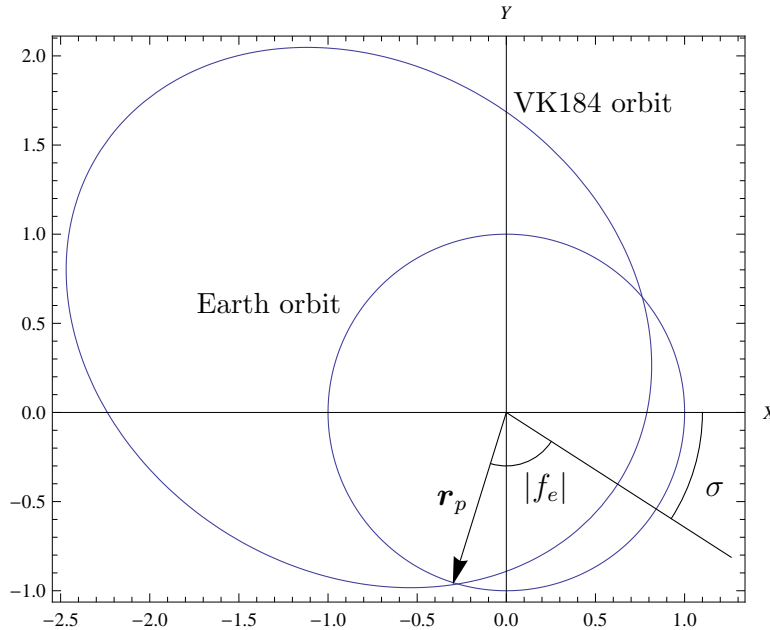


Figure 17: Heliocentric orbits of Earth and Asteroid 2007 VK184.

have from the equation of path (cf. [22]) that

$$r_e = \frac{a(1 - e^2)}{1 + e \cos f_e} \quad (132)$$

where r_e is the radius of Earth's orbit, a is the semimajor axis of the asteroid's orbit, and e is the eccentricity of the asteroid's orbit. Thus

$$f_e = \cos^{-1} \left(\frac{1}{e} \left(\frac{a(1 - e^2)}{r_e} - 1 \right) \right) \quad (133)$$

or

$$f_e = -1.3 \text{ rad} \quad (134)$$

The deflection of the asteroid for various parameter values will be calculated using (86). Thus we start by calculating the various quantities that are needed in that equation.

The velocity of the asteroid at encounter is obtained from the energy equation

$$v_{ae} = \sqrt{2 \left(\frac{\mu_s}{r_E} - \frac{\mu_s}{2a_a} \right)} \quad (135)$$

or

$$v_{ae} = 35500 \text{ m/s} \quad (136)$$

which from (35) gives for κ

$$\kappa = 1.528 \times 10^{-4} \text{ s/m} \quad (137)$$

to be used in (88). The flight path angle γ (cf. [22]) for the asteroid at the time of encounter can now be calculated from the expression for the angular momentum, (cf. [22])

$$h = r v_{ae} \cos \gamma = \sqrt{a(1 - e^2) \mu_s} \quad (138)$$

or

$$\gamma = \cos^{-1} \frac{\sqrt{a(1 - e^2) \mu_s}}{r v_{ae}} \quad (139)$$

or

$$\gamma = 0.44 \text{ rad} \quad (140)$$

Next referring to Figure 18 we calculate the magnitude of the relative velocity of the asteroid with respect to Earth as

$$v_{a/E} = \sqrt{v_E^2 + v_a^2 - 2v_a v_E \cos \gamma} \quad (141)$$

or

$$v_{a/E} = 15,200 \text{ m/s} \quad (142)$$

It then follows for the incidence angle ψ that

$$\frac{v_{a/E}}{\sin \gamma} = \frac{v_E}{\sin \psi} \quad (143)$$

or after solving for ψ

$$\psi = 0.829 \text{ rad} \quad (144)$$

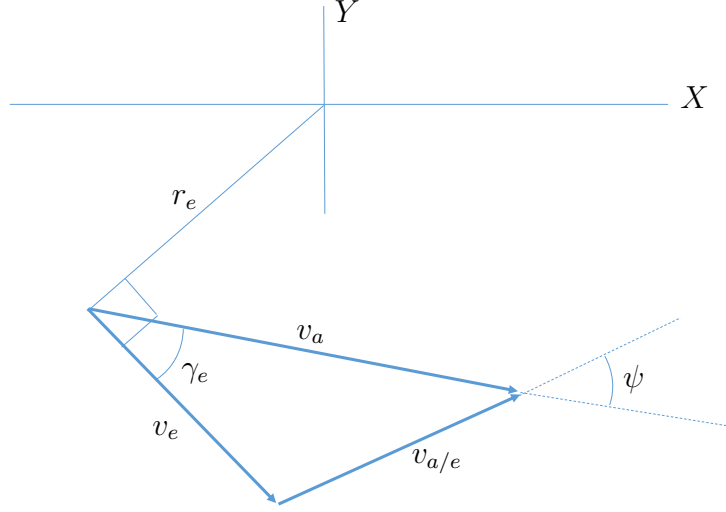


Figure 18: Geometry of the encounter of Earth and VK184 in June 2048.

For the gravity tractor, we assume a gross mass of $m_{c1} = 1500$ kg and a fuel mass of $m_f = 450$ kg. (As will be seen below, this corresponds to a mission duration of about 6 years). Following [15] the specific impulse of the spacecraft will be assumed to be $I_{sp} = 2500$ s.

From Figure 12 we pick $\theta_b = 1$ rad for a time of flight of around 1 TU. From Figure 11 we pick for simplicity $e = 0$ for $\eta_k \approx 0.8$. Using (92) we calculate the smallest radius that satisfies the plume impingement constraint to be $r_{pm} = 69.2$ m. Using (94) the time of flight on the orbit segment is then calculated to be

$$\Delta t = 2452\text{s}, \quad (145)$$

and using (114) the required Δv at the ends of the segment are calculated to be

$$\Delta v = 0.1128\text{m/s} \quad (146)$$

This value of Δv used in (87) gives

$$q = 4.602 \times 10^{-6} \quad (147)$$

The value of N is calculated based on how many times the impulsive thrusts can be imparted before all the fuel is expended, or

$$m_{c1} - m_f = m_{c1} e^{-qN} \quad (148)$$

or

$$N = -\frac{1}{q} \ln \left(\frac{m_{c1} - m_f}{m_{c1}} \right) \quad (149)$$

which yields

$$N = 77,510 \quad (150)$$

The total duration of a mission t_m is therefore

$$t_m = N \Delta t \quad (151)$$

or $t_m = 6.03$ years. Next using (83) we find

$$\lambda = 3.87 \times 10^{-5} \text{ m/s}^2 \quad (152)$$

Lastly we note that the velocity v_{ai} needs to be determined for each value of the index i . Thus for a given i we start by solving Kepler's equation for the corresponding eccentric anomaly E_i using the known eccentric anomaly at the time of encounter E_e

$$t_i - t_e = \sqrt{\frac{a^3}{\mu_s}} (E_i - E_e - e(\sin(E_i) - \sin(E_e))) \quad (153)$$

Using E_i we calculate the corresponding radius r_i from the equation of path (see [24])

$$r_i = a_a(1 - e \cos E_i) \quad (154)$$

which can be used in the energy equation to yield

$$v_{ai} = \sqrt{2 \left(\frac{\mu_s}{r_i} - \frac{\mu_s}{2a_a} \right)} \quad (155)$$

The above numerical values can now be used in (86) for a range of values of the starting time before the time of projected encounter $t_s - t_e$. For each value of i in (86) the corresponding value of v_{ai} is determined through a numerical solution of Kepler's equation (see to yield the total deflection as a function $t_s - t_e$. The result is depicted in Figure 19 (solid line).

We next consider a spacecraft of the same gross and fuel masses as above, this time deployed as a stationary gravity tractor. As the mass of the spacecraft decreases the thrust decreases in order for the spacecraft to remain at equilibrium in its stationary position. While other scenarios are possible (such as a decreasing altitude for a constant gravitational force) this is the most efficient approach as discussed in [32].

Thus it follows from (122) that the thrust required to keep the spacecraft at equilibrium also decreases according to the relation

$$T = \frac{Gm_a m_c}{2\alpha^2 r_a^2 \cos(\beta_0 + \varphi)} \quad (156)$$

Now using (156) in (123) and recalling $2dm' = dm_c$ gives

$$\frac{dm_c}{dt} = -\frac{2T}{I_{sp}g_0} \quad (157)$$

or

$$\frac{dm_c}{dt} = -\frac{Gm_a m_c}{I_{sp}g_0 \alpha^2 r_a^2 \cos(\beta_0 + \varphi)} \quad (158)$$

Solving this differential equation we have

$$m_c = m_{c1} e^{-Q(t-ts)} \quad (159)$$

where we have defined the parameter Q through

$$Q = \frac{Gm_a}{I_{sp}g_0 \alpha^2 r_a^2 \cos(\beta_0 + \varphi)} \quad (160)$$

and where m_{c1} is the mass of the spacecraft at the initial time t_s , i.e. the same initial mass as for the Keplerian gravity tractor.

To obtain the deflection caused by the stationary gravity tractor we can directly use (60):

$$\Delta\zeta^c = -\kappa \int_{t_s}^{t_f} (t_e - t) v_a \frac{Gm_{c1} e^{-Q(t-t_s)}}{\alpha^2 r_a^2} dt \quad (161)$$

We start by calculating Q using (160) which yields

$$Q = 4.50 \times 10^{-9} /s \quad (162)$$

Next from (159) we find that the longest the stationary gravity tractor can operate is

$$t_f - t_s = -\frac{1}{Q} \ln \left(\frac{m_{c1} - m_f}{m_{c1}} \right) \quad (163)$$

or

$$t_f - t_s = 2.51 \text{ years} \quad (164)$$

The integral in (161) is now evaluated numerically taking into account the variation of v_a with time according to (153)-(154). Thus we calculate the deflection created at the time of encounter for a range of values of the starting time before the projected encounter $t_s - t_e$. The results using $\alpha = 1.5$ and $\alpha = 2.5$ are shown in Figure 19: dashed line and dashed-dotted line, respectively.

Lastly, we determine the deflection created by a displaced-orbit gravity tractor of the same initial mass. Using (67) (with $m' = m$ as there is only one thruster) and (71)

$$\frac{dm_c}{dt} = -0.21 \frac{Gm_a m_c}{I_{sp} g_0} \quad (165)$$

or

$$m_c = m_{c1} e^{-Q_d(t-t_s)} \quad (166)$$

where

$$Q_d = 0.21 \frac{Gm_a}{I_{sp} g_0} \quad (167)$$

The value of Q_d is obtained to be

$$Q_d = 4.46 \times 10^{-10} /s \quad (168)$$

Next, from (166), the longest the gravity tractor can operate is found to be

$$t_f - t_s = -\frac{1}{Q_d} \ln \left(\frac{m_{c1} - m_f}{m_{c1}} \right) \quad (169)$$

or

$$t_f - t_s = 25.3 \text{ years} \quad (170)$$

Next, using we use (34) we note that the total deflection at time t_e may be written as

$$\Delta\zeta^d = -0.21\kappa \int_{t_s}^{t_f} (t_e - t) v_a \frac{Gm_{c1} e^{-Q_d(t-t_s)}}{r_a^2} dt \quad (171)$$

The integral in (171) is evaluated numerically for a range of values of the starting time before the projected encounter $t_s - t_e$. The result is shown in Figure 19 (dotted line).

In summary it is clear that the Keplerian gravity tractor can result in a deflection that is significantly larger than that for a stationary gravity tractor for a given lead time and initial mass of the spacecraft. The added deflection ranges from about 1000 km for a deployment 6 years ahead of the projected time of encounter, to more than 1500 km for a deployment 12 years ahead of the time of encounter. Recalling the discussion in the previous section, this result may be explained by the larger average force that can be exerted by the Keplerian gravity tractor as well as its overall higher fuel efficiency.

Another interpretation of Figure 19 is in terms of what lead time is necessary for a given deflection. Thus we note for example that in order to realize a deflection of 1000 km, the stationary gravity tractor would need a 13-year lead time, about twice what would be required for the Keplerian gravity tractor (about 6.5 years).

The result in Figure 19 may also be compared to a similar result in [15] where an example of an optimized stationary gravity tractor with slightly larger mass is discussed. It is seen that the deflections resulting from the Keplerian gravity tractor are of the same order of magnitude as that of the optimized stationary gravity tractor, despite the smaller initial mass of the spacecraft.

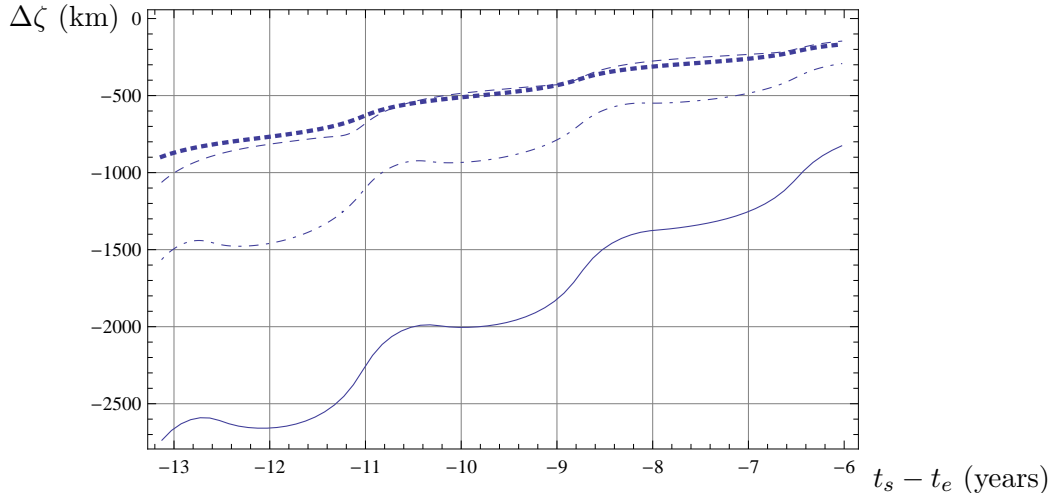


Figure 19: Comparison of deflections obtained by using the Keplerian gravity tractor (solid line); the stationary gravity tractor: $\alpha = 1.5$: (dashed line), $\alpha = 2.5$: (dashed-dotted line) as functions of the start time before the projected encounter.

7 Conclusions

While the probability of a major asteroid impact is small, its potential for severe consequences on Earth makes it worthwhile to study possible methods of deflection or impact mitigation. Asteroid deflection methods based on gravitational coupling constitute a promising approach for averting a collision. A central challenge associated with these methods is that the magnitude of the force that can be exerted using a spacecraft is generally small which means that a significant deflection

requires a large lead time.

The asteroid deflection scheme based on Keplerian orbits described in this paper addresses this issue and describes a method for a more efficient gravity tractor in terms of an increased force on the asteroid for a given mass of a spacecraft. In addition better performance is attained with regards to fuel consumption. Further, the dynamic nature of the gravity tractor makes it possible for the simultaneous deployment of several spacecraft which could decrease the time required for a given deflection.

Additional enhancement of the efficiency of the Keplerian gravity tractor can be expected through an optimization of its operation. As in [15] this would mean that the spacecraft would be in a “tugging” mode, i.e. in restricted Keplerian motion, only when the velocity of the asteroid is sufficiently large to warrant the fuel expenditure. At other times the spacecraft would simply orbit the asteroid without imparting a net impulse over time. Thus the optimized gravity tractor is especially suited for asteroids on highly elliptic orbits where a large variation in asteroid velocity occurs. The details of this approach are the subject of current work.

References

- [1] Chapman, C. R., and Morrison, D., “Impact on the Earth by Asteroids and Comets: Assessing the Hazard,” *Nature (London)*, Vol. 367, No. 6458, 1994, pp. 33-39.
- [2] Binzel, R. P., “The Torino Impact Hazard Scale,” *Planetary and Space Science*, Vol. 48, No. 4, 2000, pp. 297-303.
- [3] Izzo, D., Olympio, J., and Yam, C., “Asteroid Deflection Theory: Fundamentals of Orbital Mechanics and Optimal Control”, *1st IAA Planetary Defense Conference, Granada, Spain, 27-30 April 2009*.
- [4] Sanchez, P., Colombo, C., Vasile, M., and Radice, G., “Multicriteria Comparison Among Several Mitigation Strategies for Dangerous Near- Earth Objects,” *Journal of Guidance, Control, and Dynamics*, Vol. 32, No. 1, 2009, pp. 121V142. doi:10.2514/1.36774
- [5] Ahrens, T. J., and Harris, A. W., “Deflection and Fragmentation of Near-Earth Asteroids,” *Nature (London)*, Vol. 360, No. 6403, 1992, pp. 429-433.
- [6] Dearborn, D. S. P., Patenaude, S., and Managan, R.A., “The Use of Nuclear Explosives To Disrupt or Divert Asteroids,” in *proceedings of the Planetary Defense Conference*, <http://www.aero.org/conferences/planetarydefense/2007papers/S2-2-Patenaud-Brief.pdf>, (2007).
- [7] Hanrahan, R., “Nuclear Explosives for NEO Deflection,” *Presentation to National Research Council Committee to Review Near-Earth Object Surveys and Hazard Mitigation Strategies: Mitigation Panel*, (2009)
- [8] McInnes, C. R., “Deflection of Near-Earth Asteroids by Kinetic Energy Impacts from Retrograde Orbits,” *Planetary and Space Science*, Vol. 52, No. 7, 2004, pp. 587V590.

- [9] Dachwald, B., and Wie, B., Solar Sail Trajectory Optimization for Intercepting, Impacting, and Deflecting Near-Earth Asteroids, AIAA Paper 2005-6176, Aug. 2005
- [10] Izzo, D., Bourdoux, A., Walker, R., and Ongaro, F., “Optimal Trajectories for the Impulsive Deflection of NEOs,” IAC Paper 05- C1.5.06, 2005.
- [11] Asphaug, E., Ostro, S. J., Hudson, R. S., Scheeres, D. J., and Benzi, W., Disruption of Kilometre-Sized Asteroids by Energetic Collisions, *Nature* (London), Vol. 393, No. 6684, 1998, pp. 437V440.
- [12] Lu, E. and Love, S. “Gravitational Tractor for Towing Asteroids”, *Nature*, **438**, No. 7065, 2005, pp. 177-178
- [13] Gehler, M., Ober-Blobaum, S., Dachwald, B., and Marsden, J., “Optimal Control of Gravity Tractor Spacecraft Near Arbitrarily Shaped Asteroids,” 1st IAA Planetary Defense Conference, Granada, Spain, 27V30 April 2009.
- [14] Wie, B., “Dynamics and Control of Gravity Tractor Spacecraft for Asteroid Detection,” *Journal of Guidance, Control, and Dynamics*, Vol. 31, No. 5, 2008, pp. 1413-1423. doi:10.2514/1.32735
- [15] Olympio, J.T., “Optimal Control of Gravity-Tractor Spacecraft for Asteroid Deflection”, *Journal of Guidance Control and Dynamics*, **33**, 3, May-June 2010-, pp. 615-621.
- [16] Fahnestock, E.G., Scheeres, D.J., “Dynamic Characterization and Stabilization of Large Gravity-Tractor Designs”, *Journal of Guidance Control and Dynamics*, **31**, 3, May-June 2008, pp. 501-621.
- [17] McInnes, C., “Near Earth Object Orbit Modification Using Gravitational Coupling,” *Journal of Guidance, Control, and Dynamics*, Vol. 30, No. 3, 2007, pp. 870-873. doi:10.2514/1.25864
- [18] McInnes, C., “Dynamics, Stability, and Control of Displaced Non-Keplerian Orbits,” *Journal of Guidance, Control, and Dynamics*, Vol. 21, No. 5, 1998, pp. 799-805.
- [19] Gong, S., Li, J., BaoYin, H., “Formation flying solar-sail gravity tractors in displaced orbit for towing near-Earth asteroids”, *Celestial Mechanics and Dynamical Astronomy*, Vol. 105, 1-3, 2009, pp 159-177.
- [20] Greenwood, D. T., “Principles of Dynamics”, 2nd. ed., Prentice Hall, 1988, Chap. 4, p. 172.
- [21] Lipschutz, S., Liu, J., Spiegel, M., “Mathematical Handbook of Formulas and Tables”, 4th ed., McGraw-Hill, 2013, p. 134.
- [22] Curtis, H. D., “Orbital Mechanics for Engineering Students”, 3rd ed., Elsevier Ltd., 2014, Chap. 2
- [23] Prussing, J. E. and Conway, B. A., “Orbital Mechanics”, 2nd. ed., Oxford University Press, 2013, Chap. 1

- [24] Curtis, H. D., “Orbital Mechanics for Engineering Students”, 3rd. ed., Elsevier Ltd., 2014, Chap. 3
- [25] Prussing, J. E. and Conway, B. A., “Orbital Mechanics”, 2nd. ed., Oxford University Press, 2013, Chap. 2
- [26] Broschart, S.B. and Scheers, D.J., “Control of Hovering Spacecraft Near Small Bodies: Application to Asteroid 25143 Itokawa,” *Journal of Guidance, Control, and Dynamics*, Vol. 28, No. 2, 2005, pp. 343-354
- [27] Bate, R. R., Mueller, D. D., White, J. E., “Fundamentals of Astrodynamics”, Dover Publications Inc., 1971, Chap. 1
- [28] Curtis, H. D., “Orbital Mechanics for Engineering Students”, 3rd. ed., Elsevier Ltd., 2014, Chap. 6
- [29] JPL Small-Body Database: 2007 VK184: <http://ssd.jpl.nasa.gov/sbdb.cgi?sstr=3394541#elem>, Retrieved 2016-09-28.
- [30] NASA Near Earth Object Program: <https://web.archive.org/web/20131017014439/http://neo.jpl.nasa.gov/> Retrieved 2016-9-28.
- [31] Hale, Francis J., “Introduction to Space Flight”, Prentice Hall (1994) Chap. 8
- [32] Sanchez, J.P., Colombo, C., Vsdilr, M., and Radices, G, “Multicriteria Comparison Among Several Mitigation Strategies for Dangerous Near-Earth Objects”, *Journal of Guidance, Control, and Dynamics*, **32**-1, (2009)